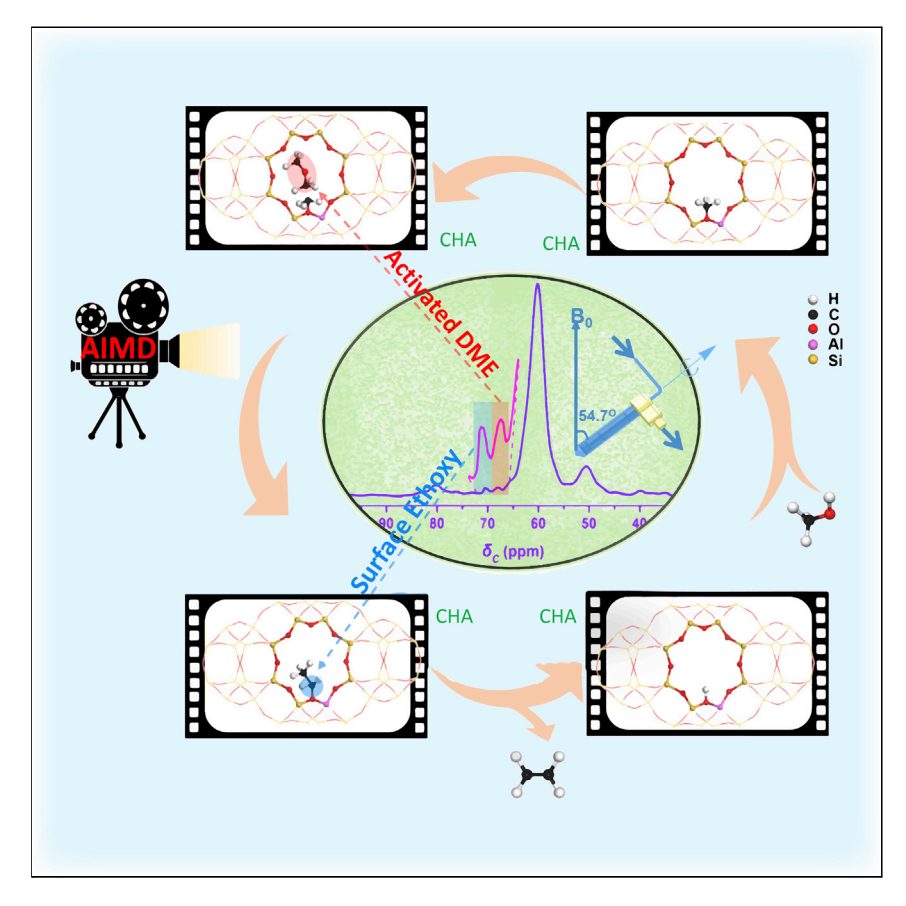




#### **Article**

# The first carbon-carbon bond formation mechanism in methanol-to-hydrocarbons process over chabazite zeolite



As a highly controversial and critical issue in C1 chemistry, the first C–C bond formation mechanism in methanol-to-hydrocarbons (MTH) reaction has attracted tremendous attention from academia. By employing *in/ex situ* solid-state NMR spectroscopy and advanced theoretical calculation technology, new insights into the first C–C bond formation mechanism were provided, resulting in a complete synergetic process with a visualized dynamic scene over an acidic zeolite catalyst.

Tantan Sun, Wei Chen, Shutao Xu, ..., Xiangju Meng, Yingxu Wei, Zhongmin Liu

xushutao@dicp.ac.cn (S.X.) zhenganm@wipm.ac.cn (A.Z.) weiyx@dicp.ac.cn (Y.W.) liuzm@dicp.ac.cn (Z.L.)

#### Highlights

SES was directly captured over zeolite catalyst in a real MTH reaction

Complete and reasonable direct C-C bond formation processes were established

A visualized process was demonstrated to reveal the dynamic scene of C–C bond coupling





Sun et al., Chem 7, 1–14 September 9, 2021 © 2021 Elsevier Inc. https://doi.org/10.1016/j.chempr.2021.05.023

## Chem



#### **Article**

## The first carbon-carbon bond formation mechanism in methanol-to-hydrocarbons process over chabazite zeolite

Tantan Sun,<sup>1,4,6</sup> Wei Chen,<sup>2,6</sup> Shutao Xu,<sup>1,\*</sup> Anmin Zheng,<sup>2,\*</sup> Xinqiang Wu,<sup>1</sup> Shu Zeng,<sup>1,4</sup> Nan Wang,<sup>1,4</sup> Xiangju Meng,<sup>5</sup> Yingxu Wei,<sup>1,\*</sup> and Zhongmin Liu<sup>1,3,7,\*</sup>

#### **SUMMARY**

The first C-C bond formation mechanism in the methanol-to-hydrocarbons (MTH) process has always been a highly controversial issue. Using solid-state NMR spectroscopy, the initial C1 reactants and C1 intermediates were observed on the HSSZ-13 zeolite surface. In particular, for the first time, the highly reactive ethene precursor, surface ethoxy species, was directly captured under a real MTH reaction. These findings and in situ captured activated C1 reactants linked C1 species and initially generated ethene, in which C1 intermediates activate methanol/DME to form the first C-C bond. For such a difficult-to-detect and extremely initial reaction process, the advanced ab initio molecular dynamics technology simulated the complete process from C1 reactants to product. The visualized reaction process vividly shows methanol/DME in the gas phase approaching SMS/TMO on zeolite, being activated via effective collision and methylation to generate an ethene precursor. The zeolite catalyst and active C1 intermediates contribute together to the first C–C bond formation in a synergistic manner.

#### **INTRODUCTION**

As the most successful non-petrochemical route for producing olefins and synthetic fuel, the methanol-to-hydrocarbons (MTH) process, especially over a chabazite (CHA) SAPO catalyst, has attracted enormous attention. <sup>1,4,6</sup> In the past few decades, considerable efforts have been devoted to the reaction mechanism of the MTH process and proposed many opinions. However, the formation of the first C–C bond is still under debate. Although at least 20 distinct direct mechanisms that explain the formation of light olefins have already been proposed since the 1970s, <sup>2,3,5,7–9</sup> none of them are acceptable because of the lack of experimental support and unrealistically high computed energy barriers. <sup>4</sup> In the 1990s, an indirect hydrocarbon pool (HCP) mechanism, which avoids high energy barriers, was proposed to explain the generation of olefins with a highly efficient reaction period. <sup>1,4,6,10,11</sup> This mechanism, however, cannot account for the formation of the first C–C bond and the origin of HCP species.

As early as 2003, Hunger and co-workers found that surface methoxy species (SMS) had high reactivity for hydrocarbon generation and proposed that SMS contributed to the formation of the first C–C bond. <sup>12</sup> Comparatively, Haw et al. proposed the presence of traces of impurities in reactants, carrier gas, and catalysts, which resulted in the first C–C bond formation and acted as the precursors of HCP species. <sup>13–16</sup> The controversies of the first C–C bond formation stem from the lack of

#### The bigger picture

Revealing the whole first C-C bond formation processes in methanol-to-hydrocarbons (MTH) reaction based on in situ spectroscopic evidence with theoretical support for the direct observation of activated C1 reactants and the highly reactive olefin precursor surface ethoxy species (SES). Herein, the complete and reasonable C-C bond formation processes were established by linking the elementary steps on the basis of these critical findings. Feasible pathways with reasonable energy barriers were explored and the real scene of these dynamic C-C bond coupling processes was visualized by the advanced ab initio molecular dynamics (AIMD) simulations.





time-resolved, sensitive experimental techniques and appropriate theoretical calculations. Recently, based on the development of spectroscopic methods and theoretical studies, new progress has been reported in revealing the direct pathway of the first C-C bond formation, which brought new insight into a direct C-C bond coupling mechanism. 17-23 The critical role of extra-framework Al (EFAL)-based Lewis acid site (LAS) in zeolites was demonstrated in the first C-C bond formation step via an Al-oxonium ion, SMS bonded to an EFAL or Al-COH<sub>2</sub><sup>+</sup> intermediates by Sautet et al., <sup>17</sup> Deng et al., <sup>18</sup> and Zheng et al., <sup>19</sup> respectively. As suggested by Fan and co-workers, 20 methanol and dimethyl ether (DME) can be activated by the methoxymethyl cation (CH<sub>3</sub>OCH<sub>2</sub><sup>+</sup>) intermediate to form C-C bond containing species. In 2016, Lercher and Weckhuysen postulated that the carbonylation of SMS by carbon monoxide (CO) can produce the framework-bound acetyl group (Zeo-COCH<sub>3</sub>), which is responsible for the yield of initial olefins. <sup>21,22</sup> In our recent study, a new NMR signal that was attributed to a surface methyleneoxy analog species, originating from DME in its activated state, was successfully captured on HZSM-5 under a real MTH condition. Based on direct evidence for the C1 reactants activation, a reliable reaction pathway—SMS/trimethyloxonium (TMO)-mediated conversion of methanol/DME into initial olefins—was proposed.<sup>23</sup> Despite these encouraging findings, more evidence, such as active intermediates and precursor species of the initial olefins are still required for linking the elementary steps to establish a complete and reasonable reaction pathway. Moreover, theoretical simulations have always been expected to present a visualized scene of the reaction process from C1 species to form a C-C bond (Figure 1).

In this work, with the aid of multiple techniques, methanol conversion over CHA zeolite catalyst, HSSZ-13, has been fully studied. Accompanied by the capture of the intermediates SMS and TMO, C1 reactant activation was detected by *in situ* solid-state NMR spectroscopy. More importantly, for the first time, the highly reactive ethene precursor, surface ethoxy species (SES), was directly captured over the catalyst in the real MTH reaction. Advanced *ab initio* molecular dynamic (AIMD) was employed to present the dynamic reaction mechanism under reaction conditions, and a visualized dynamic process was successfully demonstrated to reveal the complete reaction pathway of the C1 species coupling to form the first C–C bond.

#### **RESULTS**

#### Experimental evidence for the first C-C bond formation

The MTH reaction was carried out in a fixed-bed quartz tubular reactor under atmospheric pressure (see experimental procedures) after feeding methanol onto the HSSZ-13 (Si/Al = 15, X-ray diffraction [XRD] and scanning electron microscropy [SEM] results are shown in Figures S1 and S2) catalyst bed for a very short time (0–80 s) at 300°C, the effluents were detected by online gas chromatography. The detection of ethene and propene ahead of the appearance of methanol and DME in effluent suggests that the initially fed methanol and its dehydrated product DME stayed on the surface of HSSZ-13 as strongly adsorbed species until methanol was fed in excess (Figure S3 and Note S1). Moreover, the preferential formation of ethene over propene indicates that ethene is the first C–C bond containing product in MTH reaction.

To explore the formation mechanism of the first C–C bond over zeolite catalyst, ex situ <sup>13</sup>C CP/magic-angle spinning (MAS) NMR measurements for the <sup>13</sup>C-methanol-reacted catalysts, after reaction at varied temperatures and being quenched with

<sup>1</sup>National Engineering Laboratory for Methanol to Olefins, Dalian National Laboratory for Clean Energy, iChEM (Collaborative Innovation Center of Chemistry for Energy Materials), Dalian Institute of Chemical Physics, Chinese Academy of Sciences, Dalian 116023, China

<sup>2</sup>State Key Laboratory of Magnetic Resonance and Atomic and Molecular Physics, National Center for Magnetic Resonance in Wuhan, Wuhan Institute of Physics and Mathematics, Innovation Academy for Precision Measurement Science and Technology, Chinese Academy of Sciences, Wuhan 430071, China

<sup>3</sup>State Key Laboratory of Catalysis, Dalian Institute of Chemical Physics, Chinese Academy of Sciences, Dalian 116023, China

<sup>4</sup>University of Chinese Academy of Sciences, Beijing 100039, China

<sup>5</sup>Department of Chemistry, Zhejiang University, Hangzhou 310028, China

<sup>6</sup>These authors contributed equally

<sup>7</sup>Lead contact

\*Correspondence: xushutao@dicp.ac.cn (S.X.), zhenganm@wipm.ac.cn (A.Z.), weiyx@dicp.ac.cn (Y.W.), liuzm@dicp.ac.cn (Z.L.) https://doi.org/10.1016/j.chempr.2021.05.023





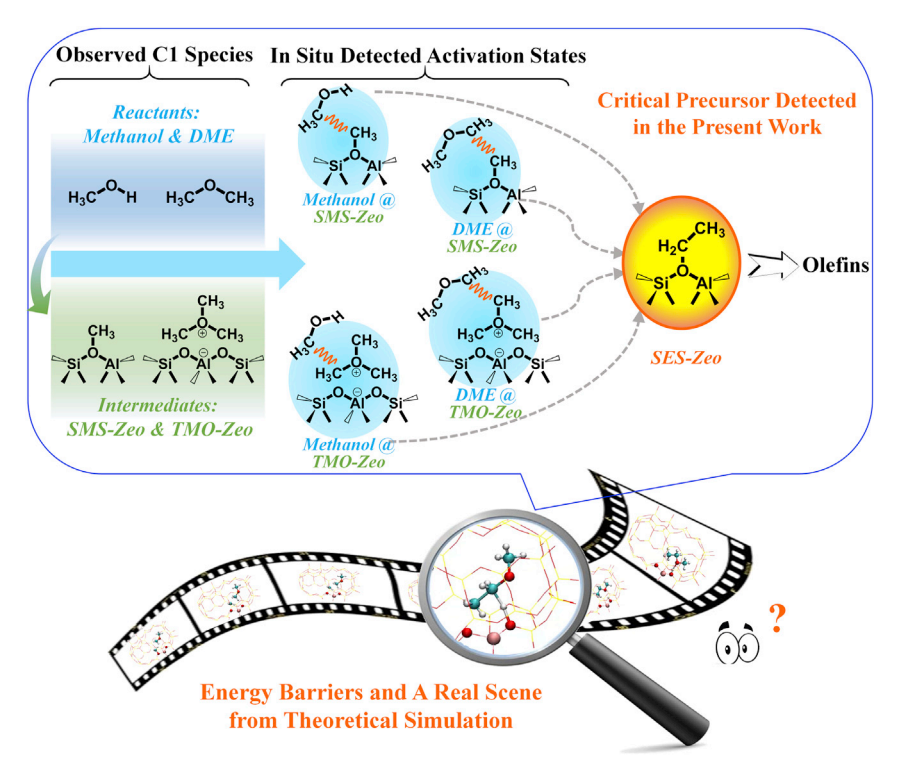


Figure 1. Schematic reaction pathway for the initial olefin formation from C1 species in methanol conversion

Starting from C1 reactants methanol/DME and C1 intermediates SMS/TMO, SES, a C–C bond containing intermediate as the ethene precursor, can be formed via *in situ*-detected activation states. Olefins will be generated by the decomposition and elimination of SES from the zeolite catalyst surface. For the process of C–C bond formation, theoretical simulations that can give complete reaction pathways with feasible energy barriers and present a real scene have always been expected.

liquid nitrogen, were conducted, and the spectra were recorded, as shown in Figure 2. At the temperature of 220°C, the first 1 min <sup>13</sup>C-methanol conversion gave rise to four signals assigned to surface-adsorbed methanol/DME (50.2 and 60.5 ppm) and surface-bound SMS/TMO (58.5 and 80.1 ppm) over HSSZ-13, respectively. 18 However, by continuously feeding 13C-methanol onto HSSZ-13 zeolite for 2 min, apart from trace amounts of cycloalkanes or oligomerized olefins at 20-30 ppm, two new signals at 70.5 and 14.2 ppm at very low intensities were simultaneously captured (see insets in Figure 2). Generally, these two signals are attributed to the methylene (-CH<sub>2</sub>-) and methyl C (-CH<sub>3</sub>) atoms of SES, respectively. <sup>24–26</sup> It is known that the ethene precursor, SES, is of very high reactivity, from which ethene can be eliminated easily. However, owing to this issue, the direct capture of SES under the reaction condition has been a huge challenge. Previous studies in the observation of SES on acidic zeolites were realized in an indirect way by the adsorption of either ethanol or CH<sub>3</sub>CH<sub>2</sub>I. <sup>24–27</sup> Accordingly, for this critical species containing initial C-C bond, there are still no reports involving direct observation of SES in real methanol conversion. For the confirmation of the formation and the direct capture of SES in the <sup>13</sup>C-methanol reaction, <sup>13</sup>C<sub>2</sub>-ethanol dehydration reaction was conducted over HSSZ-13, and the generated SES gave consistent signals in the measurements of <sup>13</sup>C CP/MAS NMR and 2D <sup>13</sup>C-<sup>13</sup>C refocused INADEQUATE NMR experiments (Figures S4 and S5). This means that the initial C-C bond was successfully captured over the zeolite catalyst at this moment. Additionally, the successful capture of SES





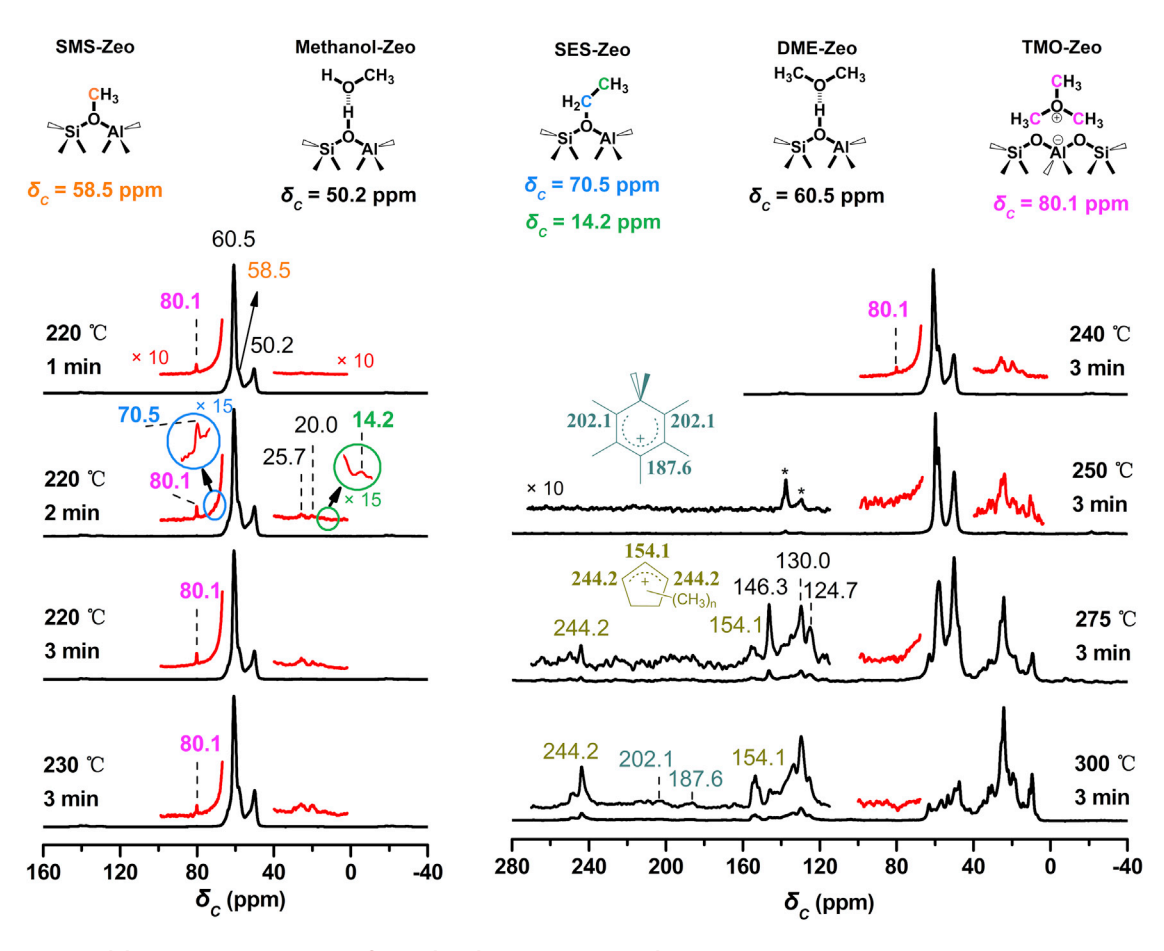


Figure 2. Ex situ solid-state NMR investigations for methanol conversion at initial MTH reaction stage

13 C CP/MAS NMR spectra of HSSZ-13 catalyst after 13 C-methanol conversion at 220° C-300° C for 1-3 min. The catalyst was quenched by liquid nitrogen after reaction and the spectra were recorded at room temperature.

not only realized the direct observation of this critical intermediate formed over zeolite in real methanol conversion for the first time but also strongly verified the existence of direct coupling of C1 species to form the C–C bond. Once ethene forms initially, the subsequent oligomerization reaction of ethene will occur to generate higher olefin/aromatic hydrocarbons as HCP species to mediate the methanol conversion via an indirect pathway.<sup>24,28</sup>

The evolution of the intermediates SMS and TMO (two important C1 intermediates) on zeolite catalyst surface during the methanol conversion at varied reaction temperatures is also clearly revealed by the <sup>13</sup>C CP/MAS NMR spectra (Figure 2). SMS and TMO were detected over HSSZ-13 at 220°C from an extremely initial MTH reaction (1 min). TMO can be formed through the coupling of SMS and DME with a low energy barrier of 88.7 kJ/mol (Figure S6). When <sup>13</sup>C-methanol was fed onto the catalyst at temperatures higher than 250°C, the signal of TMO was no longer detected. At this moment, the MTH reaction presented a highly efficient conversion with the generation and detection of HCP species, such as aromatics and cyclic carbenium ions, on the catalyst surface. The high reactivity of SMS and its critical role for initial C–C bond formation have already been emphasized. Comparatively, the significance of TMO was long overlooked owing to the unrealistically high computed energy barriers for the generation of the ethene precursor by direct deprotonation of





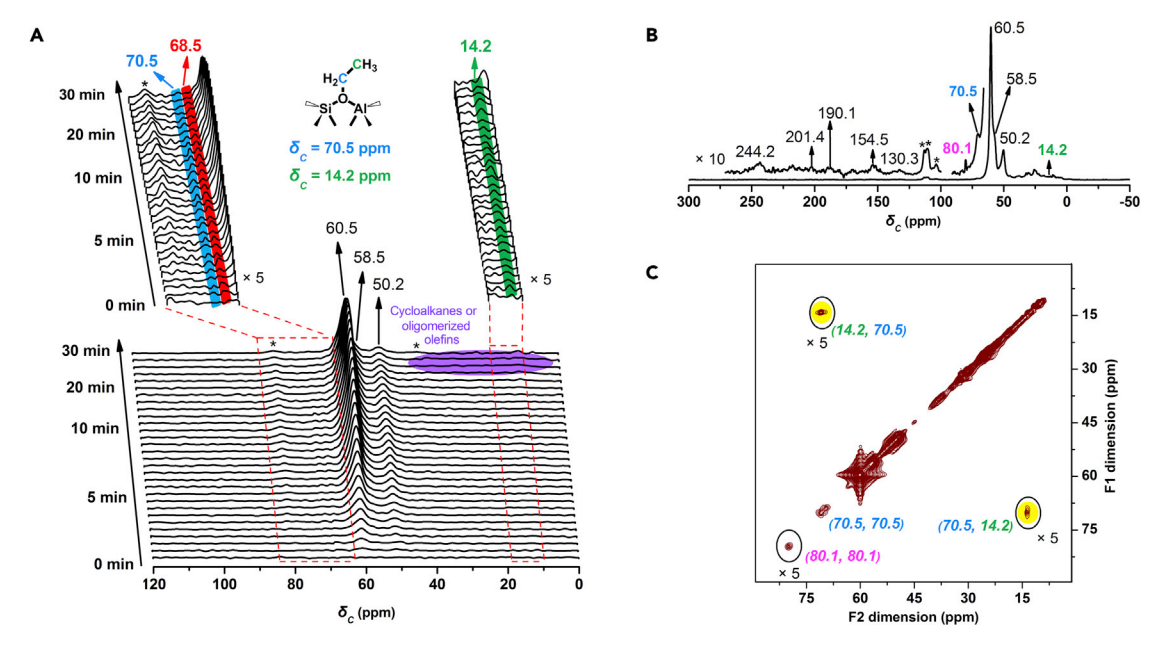


Figure 3. In situ solid-state NMR investigations for methanol conversion at initial MTH reaction stage

(A) In situ solid-state  $^{13}$ C MAS NMR spectra of HSSZ-13 with continuous-flow (CF)  $^{13}$ C-methanol conversion at 220°C. The spectra were recorded every 30 s from 0 to 10 min and then every 120 s from 10 to 30 min.

(B) The <sup>13</sup>C CP/MAS NMR spectrum of HSSZ-13 after *in situ* <sup>13</sup>C-methanol conversion at 220°C for 30 min.

(C) 2D <sup>13</sup>C CORD spin diffusion MAS NMR spectrum of the sample in (B) with a mixing time of 50 ms.

The spectra in (B) and (C) were recorded at room temperature. The asterisk symbol (\*) indicates the spinning sidebands.

TMO to form dimethyl oxonium methylide (DOMY) and further methylation to form ethyl dimethyl oxonium ion (EDMO). <sup>29–31</sup> However, a recent study found that, like SMS, TMO is also an active methylation agent and is critical for mediating methanol/DME activation over an acidic zeolite catalyst. <sup>23</sup> Herein, the evolution of the two intermediates on a catalyst surface during methanol conversion indicates that these C1 intermediates should be involved in the first C–C bond formation and play vital roles in the initial methanol conversion.

To further clarify real-time interactions and transformations of C1 species at the initial stage of our MTH reaction, in situ solid-state NMR measurements of continuous-flow (CF) <sup>13</sup>C-methanol conversion over HSSZ-13 were conducted at 220°C in a rotor reactor, and the <sup>13</sup>C MAS NMR spectra were recorded, as shown in Figure 3A. Three peaks at 50.2, 58.5, and 60.5 ppm stem from the surface-adsorbed/ bound methanol, SMS, and DME, respectively, which could be easily distinguished by real-time monitored <sup>13</sup>C MAS NMR spectroscopy. A newly emerging signal at 68.5 ppm with a very low intensity was successfully captured by in situ NMR technique. However, after an in situ <sup>13</sup>C-methanol reaction at 220°C for 30 min (Figure 3B), this peak completely disappeared in the spectrum recorded at room temperature. Considering the absence of the newly detected signal in ex situ experiments (Figure 2), we concluded that this signal can only be captured in situ and is observable at the very initial MTH reaction stage. In combination with <sup>13</sup>Cmethanol reaction over HZSM-5,23 this signal is assigned to an important surface methyleneoxy analog species originating from activated DME with an elongated C-H bond by the electrophilic attack of SMS-Zeo or TMO-Zeo.

Conducting the reaction at a relatively low reaction temperature slowed down the activation step. More importantly, this allowed successful in situ tracking of the





activation of C1 reactants and the formation of the initial C-C bond containing species over an HSSZ-13 catalyst. Two signals at 70.5 and 14.2 ppm from SES, the very important ethene precursor, which appear in the ex situ <sup>13</sup>C CP/MAS NMR spectra (Figure 2), were also successfully captured and were recorded in real time by in situ NMR spectroscopy (Figure 3A). Different from the signal assigned to the activation state of DME at 68.5 ppm, after <sup>13</sup>C-methanol conversion and after the catalyst was cooled down, the formed SES was still detectable as shown by room temperature recorded <sup>13</sup>C CP/MAS NMR and 2D <sup>13</sup>C-<sup>13</sup>C combined R2-driven (CORD) spin diffusion MAS NMR spectra (Figures 3B and 3C). The capture of the activated DME (68.5 ppm) and the formed SES (70.5 and 14.2 ppm) over the catalyst during the very initial reaction period implied that SES, as the ethene precursor containing C-C bond, is generated with the reactant activation by the C1 intermediates, such as SMS and TMO. The successful electrophilic attack from SMS or TMO to C1 reactants, monitored by in situ technique, leads to the activation and further methylation of methanol/DME. Consequently, SES could be generated over the catalyst surface in this way (Figure 1). By prolonging the reaction time, the signals of SES and activated C1 reactants were weakened after 20 min, which was then accompanied by the generation and accumulation of trace amount cyclic organics or oligomerized olefins at 20-40 ppm. This suggests the occurrence of secondary reactions of the initially formed olefin products.

The effluents of methanol conversion over HSSZ-13 at 220°C was monitored by online gas chromatography and the results are presented in Figure \$7. Similar to the results of the MTH reaction at 300°C (Figure \$3), ethene was also detected ahead of the appearance of methanol and DME. The capture of ethene as the initial C–C bond containing product in gas product at 40 s was in consistent with the *in situ* observations of activated C1 reactants and SES on catalyst surface from the very beginning of MTH reaction. Additionally, it is worth noting that propane, as an MTH product generated by hydrogen transfer reaction of initially formed olefinic species, 32 was detected at the period of 13 to 30 min, which also indicated the formation of H-unsaturated hydrocarbons. Considering the *in situ* observed cyclic organics or oligomerized olefins on a catalyst surface by NMR after 20 min, it can be inferred that the evolution of the predominant reaction route from the direct mechanism at the beginning of the reaction to the indirect route in the efficient stage of methanol conversion has been in progress during this period.

Based on the capture and confirmation of C1 intermediates (SMS and TMO) and initially generated C–C bond containing species (SES) on the catalyst surface by NMR spectroscopy, an integrated description can be proposed for the first C–C bond formation during methanol conversion. The initial C–C bond containing species was formed from the C1 reactants conversion mediated by the C1 intermediates, SMS, or TMO. The generated SES, as ethene precursor, will be decomposed quickly, and finally, the initial ethene will be eliminated from the catalyst surface. Based on a series of encouraging experimental results that point to the fact that the first C–C bond formation directly originating from C1 species, specific interactions between these C1 species will be investigated by advanced theoretical calculations to answer how the activation of the SMS or TMO successfully drives the C1 species conversion to form the C–C bond.

#### Theoretical simulations of the first C-C bond formation by AIMD

To explore the complete pathways of the first C–C bond formation in detail, advanced theoretical calculations are required. Herein, an AIMD simulation based on a meta-dynamic method was employed to present a visualized and dynamic





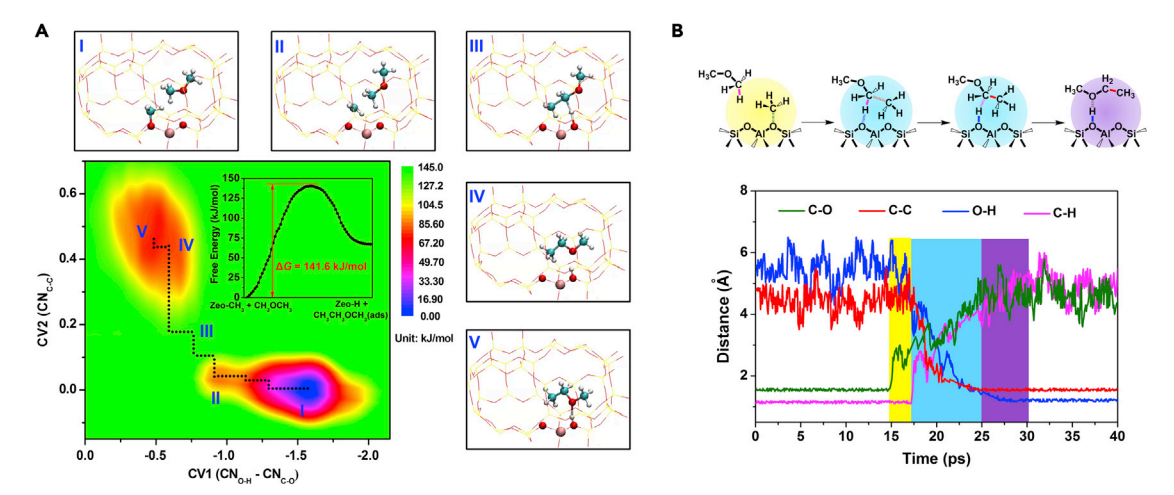


Figure 4. AIMD simulation results of the C-C bond formation starting from DME and SMS

(A) 2D free energy surface and minimal energy path of the first C–C bond formation starting from DME and SMS (insets: free energy profiles along with the minimal energy path), where  $CN_{C-C}$ ,  $CN_{O-H}$ , and  $CN_{C-O}$  are the coordination numbers of methyl C atoms between DME and SMS, methyl H atom in DME and negatively charged framework O atom, methyl C atom in SMS and its connected framework O atom, respectively.  $CN_{O-H} - CN_{C-O}$  is the difference between  $CN_{O-H}$  and  $CN_{C-O}$ . The snapshots of five representative (meta-) stable states encountered along the reaction trajectory: (I) reactant basin; (II) approaching state; (III) activation state; (IV) product state; and (V) product basin are also shown. The color codes in white, light blue, red, and pink are H, C, O, and AI, respectively.

(B) The evolution of the C-O, C-C, O-H, and C-H bond distances in the DME and SMS over HSSZ-13 zeolite with AIMD simulations.

activation/conversion processes of C1 reactants. As opposed to static DFT calculation, the AIMD simulation is not only able to evaluate the feasibility of the proposed reaction pathway but it can also visually reproduce the scene of the reaction process under experimental temperature and pressure.

Direct pathways of the first C-C bond formation in the MTH process, starting from methanol/DME with SMS or TMO as the intermediates, have been explored by AIMD simulation under reaction conditions. To estimate the reaction pathways and visualize the dynamic process, the AIMD simulation was performed with two collective variables (CVs) by the coordination numbers (CNs) of pivotal bond formation/ breakage during the reaction process. All possible combinations of methanol/DME activation mediated by either SMS or TMO were evaluated in which feasible reaction pathways with reasonable free energy barriers were explored. All these reaction pathways and free energy barriers can be produced according to the CVs: the first CV (CV1 =  $CN_{O-H} - CN_{C-O}$ ) is used to track the O–H bond formation (recovery of Brønsted acid site [BAS], generated by the H atom from methanol/DME donated to the negatively charged framework O atom of zeolite) and C-O bond breakage (C–O bond in SMS-Zeo/TMO-Zeo); the second CV (CV2 =  $CN_{C-C}$ ), as the major reaction coordination, directly manipulates the C-C bond formation (C atoms coupling between methanol/DME and SMS/TMO) (see experimental procedures for details). Moreover, 2D free energy surfaces were constructed by simulation with the combination of added Gaussian hills (Figures 4A and S8-S10). These dynamic coupling reactions are visually presented in the Videos S1, S2, S3, and S4.

To better illustrate the C–C bond formation process via direct C1 species coupling, herein, the typical pathway with the participation of DME and SMS is explicitly described as an example. As shown in Figure 4A, the 2D free energy surface of the feasible pathway is presented with five representative (meta-) stable states encountered along the C1 species conversion and C–C bond formation. At the





beginning of the process, it is illustrated in state (I) that a DME molecule is moving freely around a reactive SMS in the CHA cavity. Then, DME approaches the SMS to form state (II) followed by short-range collisions between two methyl groups of DME and SMS, which leads to DME activation. The initial C-C bond was synchronistically formed by electrophilic attack of SMS through an activation state (III), accompanied with a synergistic nucleophilic attack on the C-H bond of DME by the negatively charged framework O atom in the neighborhood. Subsequently, the C-C bond containing species, methyl ethyl ether (MEE), is generated immediately (state (IV)) and adsorbed on BAS (state (V)). Additionally, the bond distances evolution, related to the bond breakage of C-O in SMS and C-H in DME, and the bond formation of C-C between C atoms in SMS and DME and O-H between the negatively charged framework O atom and methyl H atom in DME, during the process of C-C bond formation, are sampled and displayed in Figure 4B. These bond distance evolution exhibits the formation/breakage of the typical bonds along with simulation time in an intuitive way. It can be apparently observed that the distances of C-C and O-H bonds vary irregularly near 4.5 Å and 5.7 Å, respectively, during the first 15 ps for adjusting relative configuration between DME and SMS. Notably, at the time of 15 ps, the ionic property of the methyl group in SMS is effectively enhanced with the elongation of C-O bond, and ultimately leads to C-O bond breakage of SMS from the zeolite framework. More importantly, with the approach of DME and ionic methyl group of SMSs, the initial C-C bond coupling is found to occur between the two C atoms at 17 ps. Meanwhile, one H atom in DME gradually transfers to the negatively charged framework O atom, eventually resulting in the C-H bond breakage and C-C bond formation at 25 ps. During the C-C bond formation from 17 to 25 ps, a surface methyleneoxyl analog species originating from the activated DME by the attack from SMS can be observed unambiguously, which agrees with the operando capture of the activated DME by in situ <sup>13</sup>C MAS NMR spectroscopy (Figure 3A).

On the basis of AIMD simulations, the corresponding free energy barriers for the feasible reaction pathways can be quantitatively extracted by tracking the minimal energy path on a 2D energy surface. As shown in Figure 4A, the free energy barrier for the C-C bond coupling reaction of DME and SMS over HSSZ-13 is 141.6 kJ/mol. Other feasible pathways with the participation of methanol/DME and SMS/TMO over HSSZ-13 zeolite at the same simulation condition are presented in detail in Figures 5 and S8-S10. Comparatively, when the C-C bond is formed via the SMS-mediated methanol pathway (see Path A<sub>1</sub> in Figure 5), a relatively higher barrier of 170.5 kJ/mol is predicted due to the lower nucleophilicity of methanol than that of DME.<sup>33,34</sup> As an alternative methylation agent, the generated TMO over HSSZ-13 zeolite was predicted to convert methanol and DME into ethanol or MEE with reasonable barriers of 158.7 kJ/mol (Path  $B_1$ ) and 154.4 kJ/mol (Path  $B_2$ ). The C-C bond containing species, ethanol and MEE, continued to be transformed into SES with free energy barriers of 73.6 and 98.7 kJ/mol, respectively, and finally, ethene was generated by the deprotonation of SES with a higher free energy barrier of 103.4 kJ/mol (Figures S11 and 5), which may lead to the NMR experimental observations of SES with the absence of ethanol and MEE. Furthermore, the free energy barriers of the current first C-C bond formation mechanisms were also compared with the carbonylation mechanism (Figure S12, between SMS and CO) reported before.  $^{21,22,29,35,36}$  With the consideration of the adsorption process (Tables S3 and S4), the current mechanisms of Path A2, Path B1, and Path B2 are still more preferable, while the free energy barrier of Path A<sub>1</sub> is slightly higher than that of the carbonylation mechanism. Briefly, the direct mechanisms for the first C-C bond formation involving activated reactants captured by in/ex situ NMR experiments have





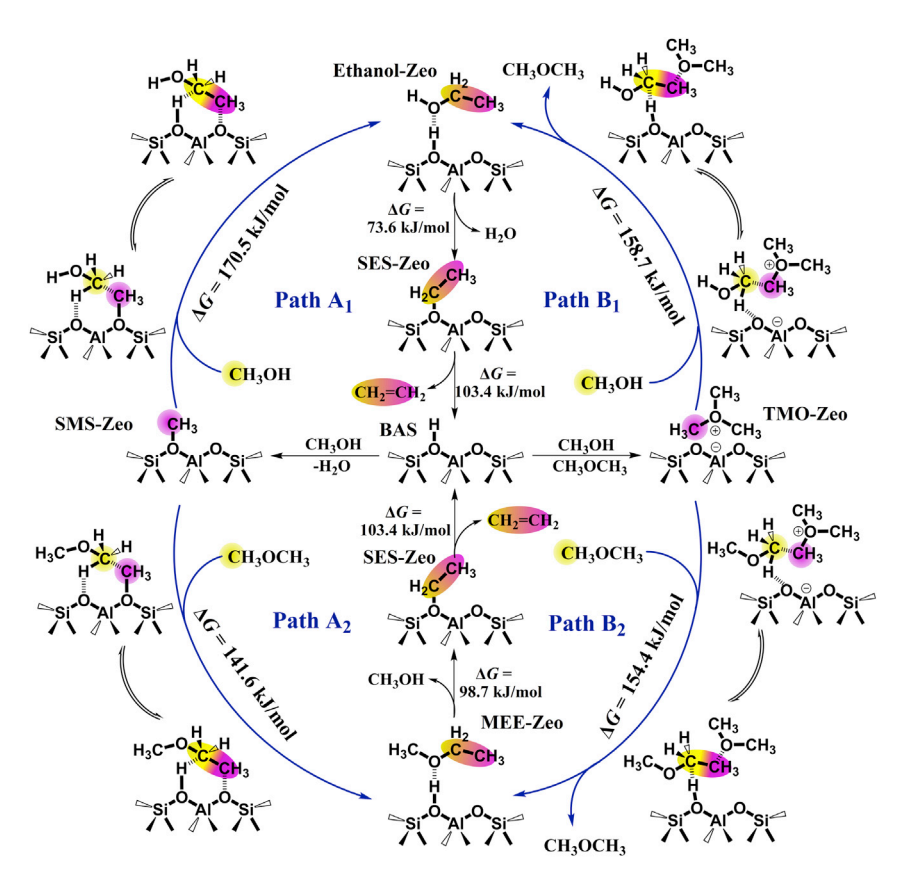


Figure 5. Plausible reaction pathways for the C-C bond formation

Catalytic cycles and the related activation barriers for the initial C–C bond formation with SMS-(left) and TMO-(right) mediated methanol (upper part) and DME (lower part) conversion on HSSZ-13 zeolite predicted by AIMD simulations. The C atoms in activated reactants, intermediates, and in methylene and methyl groups of SESs have been directly captured by *in/ex situ* solid-state NMR measurements in this work.

been theoretically determined and rationalized by AIMD simulations. Additionally, the free energy barriers reported here are smaller than those reported in previous studies, <sup>29</sup> which is majorly due to the consideration of the true vibrational nature of reaction species in AIMD simulations. To unequivocally verify the dominant C–C bond coupling mechanism, kinetic analysis of the early stages of MTH should also be considered together with the influence of diffusion, collision, and coverage for this autocatalytic process.

#### **Conclusions**

In conclusion, the first C–C bond formation during the very early stage of the MTH process was fully revealed by well-matched evidence from advanced NMR spectroscopy and AIMD simulations. For the first time, the vitally important C–C bond containing intermediate, SES as the precursor of initial ethene, was directly captured in a real MTH reaction. The simultaneous *in situ* observation of C1 intermediates (SMS and TMO), activated C1 reactants, and SES revealed the synergistic catalysis of zeolite and the formed C1 intermediates. This enabled us to describe the complete initial C–C bond formation pathways of SMS/TMO-mediated methanol/DME conversion to olefin products. Theoretical calculations by AIMD not only explored feasible pathways with reasonable energy barriers but also visualized the scene of





the dynamic C–C bond coupling process. The first C–C bond formation route, starting from DME and SMS and linking the experimentally captured surface intermediates and precursor, presented the minimal energy path along the free energy surface, which illustrates the dynamic reaction course of C–O and C–H bond breakage and C–C bond formation. The consistent experimental and theoretical results presented herein shed light on the controversial issue of the first C–C bond formation in MTH reaction.

#### **EXPERIMENTAL PROCEDURES**

#### **Resource availability**

#### Lead contact

Further information and requests for resources should be directed to and will be fulfilled by the lead contact, Professor Zhongmin Liu (liuzm@dicp.ac.cn).

#### Materials availability

This study did not generate new unique reagents.

#### Data and code availability

The published article includes all datasets generated or analyzed during this study.

#### Materials and characterization

HSSZ-13 was obtained from Zhejiang University, which was prepared according to the published method. The powder XRD pattern of HSSZ-13 was recorded using a PANalytical X'Pert PRO X-ray diffractometer with Cu K $\alpha$  radiation ( $\lambda$  = 1.5418 Å) operating at 40 kV and 40 mA. The crystallite size and morphology of the HSSZ-13 zeolite were investigated by a Hitachi SU8020 scanning electron microscope. The chemical composition of the HSSZ-13 (Si/Al = 15) was determined with a Philips Magix-601 X-ray fluorescence (XRF) spectrometer.

#### MTH conversion

The zeolite sample was first pressed into tablets, crushed, and sieved. The fraction of 40–60 mesh was chosen for MTH conversion study. MTH conversion was carried out in a fixed-bed quartz tubular reactor under atmospheric pressure at 220°C–300°C. Prior to the introduction of methanol, the catalyst was activated *in situ* at 550°C under a flow of helium (20 ml/min) for 1 h. The methanol was fed by passing helium through a saturation evaporator with a methanol weight hourly space velocity (WHSV) of  $2.0\,h^{-1}$  for 1–30 min. Then, the catalysts were quenched by liquid nitrogen and transferred to the NMR rotors quickly. The reaction products were analyzed by an online Agilent gas chromatography equipped with a HP-PLOTQ capillary column and an FID detector.

#### Solid-state NMR measurements

All solid-state NMR experiments were performed on a Bruker Avance III 600 spectrometer equipped with a 14.1 T wide-bore magnet. The resonance frequencies were 150.9 and 600.13 MHz for  $^{13}\text{C}$  and  $^{1}\text{H}$ , respectively. The ex situ  $^{13}\text{C}$  CP/MAS NMR spectra were recorded with a  $\pi/2$  pulse width of 4  $\mu s$ , a contact time of 3 ms and a recycle delay of 2 s. 1,024–40,960 scans were accumulated at a spinning rate of 12 kHz. The chemical shifts were referenced to adamantane with the upfield methine peak at 29.5 ppm. In the in situ solid-state NMR experiments, about 200 mg of pre-dehydrated HSSZ-13 was filled into a 7 mm NMR rotor reactor and pressed into a hollow cylinder with a specially constructed tool under dry Ar atmosphere in a glove box. After being transferred to the 7 mm high temperature MAS NMR probe (MAS CAT probe), the catalyst was activated at 300°C for 1 h





under flowing helium (40 ml/min), which was introduced into the spinning MAS rotor via the injection tube. Subsequently, <sup>13</sup>C-methanol was fed into the MAS NMR rotor reactor by passing the carrier gas through a <sup>13</sup>C-methanol saturator kept at  $10^{\circ}$ C with a WHSV of 1  $h^{-1}$ .  $^{13}$ C MAS NMR spectra were recorded using a one pulse sequence with a spinning rate of 3 kHz. 2D <sup>13</sup>C-<sup>13</sup>C CORD spin diffusion MAS NMR spectra was conducted on a 4 mm WVT MAS probe with a 2 s recycle delay at the spinning rate of 12 kHz. 50 ms for the spin diffusion mixing time was used. The  $\pi/2$  pulse width of <sup>1</sup>H and <sup>13</sup>C were 4.5 and 4.3  $\mu$ s at 70 and 200 W, respectively. Two-pulse phase-modulation (TPPM) <sup>1</sup>H decoupling with a radio frequency (RF) field strength of 55.6 kHz was performed during the acquisition, and continuous wave (CW) <sup>1</sup>H decoupling with the same RF field strength was applied during the t<sub>1</sub> evolution time. The 2D <sup>13</sup>C-<sup>13</sup>C INADEQUATE was conducted on a 4 mm WVT MAS probe with a spinning rate of 12 kHz and 2 s recycle delay.  $\pi/2$  pulse width of <sup>1</sup>H and <sup>13</sup>C were 4.5 and 4.3  $\mu$ s at 70 and 200 W, respectively. To obtain a better signal-to-noise ratio, the initial  $^{13}$ C signal was prepared by  $^{1}$ H  $\rightarrow$ <sup>13</sup>C CP with a contact time of 3 ms.

#### <sup>13</sup>C<sub>2</sub>-ethanol dehydration experiment

HSSZ-13 catalyst was dehydrated typically at  $420^{\circ}\text{C}$  and a pressure below  $10^{-3}$  Pa in a quartz tube for over 12 h. After catalyst dehydration, a certain amount of  $^{13}\text{C}_2$ -ethanol was introduced into the HSSZ-13 sample. The  $^{13}\text{C}_2$ -ethanol dehydration reaction was conducted at  $150^{\circ}\text{C}$  for 1 h. Then, the sample was degassed at ambient temperature for 30 min to remove physisorbed ethanol and water. Finally, the sample was transferred to the rotors for NMR tests in a glove box under dry Ar atmosphere.

#### In situ DRIFTS

In situ DRIFT spectra were collected on a Bruker Tensor 27 instrument supplied with an mercury-cadmium-telluride (MCT) detector. The catalyst powder was contained in a diffuse reflectance infrared cell with a ZnSe window. The absorbance spectra were obtained by collecting 32 scans at 4 cm $^{-1}$  resolution. Methanol was fed by passing the carrier gas (N<sub>2</sub>) through a saturation evaporator with methanol. Before the introduction of continuous-flow methanol, the sample was first calcined using an N<sub>2</sub> stream flowing at 20 ml/min at 500°C for 120 min. Subsequently, the catalyst was cooled down to 220°C under an N<sub>2</sub> stream, and the spectrum of catalyst was recorded as reference.

#### Theoretical calculation

Periodic density functional theory was opted to optimize the geometrical structures and cell parameter, and subsequently, a 5 ps NPT molecular dynamics simulation was applied to relax the structure and cell under external conditions. The formation of the first C–C bond, which is a rare event, was studied using meta-dynamics (MTD) simulations at 673 K in a canonical ensemble (NVT), based on the relaxed cell parameters from the NPT simulation. This advanced, sampling technique is used to enhance the probability of sampling chemical reactions or rare events, which requires the definition of a limited number of CV for describing the reaction coordinate. Since the coupling of first C–C bond relates to multiple bond formations and ruptures, the best CV with numerous attempts to drive the reaction pathways is described in Figure S13. The MTD simulation is biased by regularly spawning Gaussian hills along the chosen collective variable(s), which are defined by CN:





$$C N = \sum_{ij} \frac{1 - \left(\frac{r_{ij} - d_0}{r_0}\right) n}{1 - \left(\frac{r_{ij} - d_0}{r_0}\right) m}$$

in which the sum runs over two sets of atoms I and j with  $r_{ij}$ , the interatomic distance between atoms I and j, and  $r_0$ , a reference distance. In this study, the parameters  $d_0$ , n, and m are set at 0, 6, and 12, respectively. The first collective variable was defined by a difference of CNs:  $CV1 = CN_{C-O} + CN_{C-O}$  to describe proton transfer and methyl dissociation. Reference distances were 1.0 Å of CN<sub>O-H</sub> and 2.1 Å of CN<sub>C-O</sub>. The second collective variable (CV2), CN<sub>C-C</sub>, was used to describe the C-C bond formation with a reference distance of 1.5 Å. Hills with widths of 0.035 and 0.045 for CV1 and CV2 were spawned every 100 time steps, and the height of the Gaussian hills was set to 3 kJ/mol. The simulations were continued until the height of the additional hills no longer influenced the resulting free energy profile. Based on the sum of the spawned Gaussian hills, the 2D free energy profile of the reaction was reconstructed, and the lowest free energy paths (LFEP) were calculated by minimum energy pathway analysis for energy landscapes (MEPSA) software. 38 All geometrical optimizations and MD simulations were performed with a CP2K software package, using a PBE functional, including Grimme D3 dispersion corrections, a doublezeta valence polarized (DZVP) basis set, and Goedecker, Teter, and Hutter (GTH) pseudopotentials, where the time step of MD simulations was set as 0.5 fs. The hexagonal unit cell of HSSZ-13 containing 108 atoms (36T atoms) was used in this study. The complete CHA cavity in this model was used to represent the nanoreactor. To estimate possible underestimates to reaction barriers of the PBE-D3 method in static calculations, <sup>39,40</sup> the reliability of current methods in this work has been verified by comparing the adsorption energies and potential energies with hybrid functional (PBE0-D3 and B3LYP-D3) and bigger basis sets (TZVP and TZV2P) (Tables S1-S4; Figure \$14). Notably, although the PBE-D3/DZVP method reveals consistency with the results of hybrid functional and bigger basis sets, more reliable results still exist that possibly underestimate the "chemical accuracy" methods of the combination of the high level post-HF single point energy and periodic optimized structure. 39,41,42

#### **SUPPLEMENTAL INFORMATION**

Supplemental information can be found online at https://doi.org/10.1016/j.chempr. 2021.05.023.

#### **ACKNOWLEDGMENTS**

We thank the National Natural Science Foundation of China (22022202, 21991092, 21991090, 21972142, 21902153, 22032005, 22002174), National Key R&D Program of China (2018YFB0604901), Liaoning Revitalization Talents Program (XLYC1807227, XLYC1808014), Youth Innovation Promotion Association of the Chinese Academy of Sciences (2014165), Key Research Program of Frontier Sciences, Chinese Academy of Sciences (QYZDY-SSW-JSC024), and the International Partnership Program of Chinese Academy of Sciences (121421KYSB20180007) for the financial support. We thank Prof. Bučko Tomáš (Comenius University in Bratislava) and Prof. Dario Rocca (Universitéde Lorraine and CNRS) for their kind discussions on theoretical calculations.

#### **AUTHOR CONTRIBUTIONS**

T.S. and S.X. conceived, coordinated the research, and designed the experiments. W.C. and A.Z. conducted the theoretical calculation. X.W. helped in analyzing the spectra of  $ex\ situ$  and  $in\ situ$  MAS NMR. S.Z. assisted and performed the  $^{13}C_2$ -ethanol





dehydration experiment and 2D <sup>13</sup>C-<sup>13</sup>C refocused incredible natural abundance double quantum transfer experiment (INADEQUATE) NMR experiments. N.W. helped in conducting fixed-bed MTH reactions. X.M. prepared the HSSZ-13 zeolite sample. T.S., W.C., S.X., A.Z., and Y.W. contributed to writing and revising the manuscript. S.X., A.Z., Y.W., and Z.L. supervised the scientific work and led the collaborative efforts. All authors discussed the results and commented on the manuscript.

#### **DECLARATION OF INTERESTS**

The authors declare no competing interests.

Received: September 18, 2020 Revised: December 4, 2020 Accepted: May 28, 2021 Published: September 9, 2021

#### **REFERENCES**

- Tian, P., Wei, Y., Ye, M., and Liu, Z. (2015). Methanol to olefins (MTO): from fundamentals to commercialization. ACS Catal 5, 1922–1938.
- Swabb, E.A., and Gates, B.C. (1972). Diffusion, reaction, and fouling in H-mordenite crystallites. The catalytic dehydration of methanol. Ind. Eng. Chem. Fund. 11, 540–545.
- Ono, Y., and Mori, T.J. (1981). Mechanism of methanol conversion into hydrocarbons over ZSM-5 zeolite. Chem. Soc. Faraday Trans. 77, 2209–2221.
- Olsbye, U., Svelle, S., Lillerud, K.P., Wei, Z.H., Chen, Y.Y., Li, J.F., Wang, J.G., and Fan, W.B. (2015). The formation and degradation of active species during methanol conversion over protonated zeotype catalysts. Chem. Soc. Rev. 44, 7155–7176.
- Chang, C.D., and Silvestri, A.J. (1977). The conversion of methanol and other Ocompounds to hydrocarbons over zeolite catalysts. J. Catal. 47, 249–259.
- Xu, S., Zhi, Y., Han, J., Zhang, W., Wu, X., Sun, T., Wei, Y., and Liu, Z. (2017). Advances in catalysis for methanol-to-olefins conversion. Adv. Catal. 61, 37–122.
- Olah, G.A. (1981). Higher coordinate (hypercarbon containing) carbocations and their role in electrophilic reactions of hydrocarbons. Pure Appl. Chem. 53, 201–207.
- Novakova, J., Kubelkova, L., and Dolejsek, Z. (1987). Primary reaction steps in the methanolto-olefin transformation on zeolites. J. Catal. 108, 208–213.
- Tajima, N., Tsuneda, T., Toyama, F., and Hirao, K. (1998). A new mechanism for the first carboncarbon bond formation in the MTG process: a theoretical study. J. Am. Chem. Soc. 120, 8222– 8229.
- Li, J., Wei, Y., Chen, J., Tian, P., Su, X., Xu, S., Qi, Y., Wang, Q., Zhou, Y., He, Y., and Liu, Z. (2012). Observation of heptamethylbenzenium cation over SAPO-type molecular sieve DNL-6 under real MTO conversion conditions. J. Am. Chem. Soc. 134, 836–839.

- Xu, S., Zheng, A., Wei, Y., Chen, J., Li, J., Chu, Y., Zhang, M., Wang, Q., Zhou, Y., Wang, J., et al. (2013). Direct observation of cyclic carbenium ions and their role in the catalytic cycle of the methanol-to-olefin reaction over chabazite zeolites. Angew. Chem. Int. Ed. Engl. 52, 11564–11568.
- Wang, W., Buchholz, A., Seiler, M., and Hunger, M. (2003). Evidence for an initiation of the methanol-to-olefin process by reactive surface methoxy groups on acidic zeolite catalysts. J. Am. Chem. Soc. 125, 15260–15267.
- Song, W., Marcus, D.M., Fu, H., Ehresmann, J.O., and Haw, J.F. (2002). An oft-studied reaction that may never have been: direct catalytic conversion of methanol or dimethyl ether to hydrocarbons on the solid acids HZSM-5 or HSAPO-34. J. Am. Chem. Soc. 124, 3844–3845.
- Cui, Z., Liu, Q., Bain, S., Ma, Z., and Song, W. (2008). The role of methoxy groups in methanol to olefin conversion. J. Phys. Chem. C 112, 2685–2688
- Marcus, D.M., McLachlan, K.A., Wildman, M.A., Ehresmann, J.O., Kletnieks, P.W., and Haw, J.F. (2006). Experimental evidence from H/D exchange studies for the failure of direct C-C coupling mechanisms in the methanol-toolefin process catalyzed by HSAPO-34. Angew. Chem. Int. Ed. 45, 3133–3136.
- Haw, J.F., Marcus, D.M., and Kletnieks, P.W. (2006)Y. Jiang, W. Wang, V.R.R. Marthala, J. Huang, and B. Sulikowski, eds.. M. Hunger. J. Catal. 244, 130–133.
- Comas-Vives, A., Valla, M., Copéret, C., and Sautet, P. (2015). Cooperativity between Al sites promotes hydrogen transfer and carboncarbon bond formation upon dimethyl ether activation on Alumina. ACS Cent. Sci. 1, 313–319.
- Wang, C., Chu, Y., Xu, J., Wang, Q., Qi, G., Gao, P., Zhou, X., and Deng, F. (2018). Extraframework Aluminum-assisted initial C-C bond formation in methanol-to-olefins conversion on zeolite H-ZSM-5. Angew. Chem. Int. Ed. 57, 10197–10201.

- Chu, Y., Yi, X., Li, C., Sun, X., and Zheng, A. (2018). Brønsted/Lewis acid sites synergistically promote the initial C-C bond formation in the MTO reaction. Chem. Sci. 9, 6470–6479.
- Li, J., Wei, Z., Chen, Y., Jing, B., He, Y., Dong, M., Jiao, H., Li, X., Qin, Z., Wang, J., and Fan, W. (2014). A route to form initial hydrocarbon pool species in methanol conversion to olefins over zeolites. J. Catal. 317, 277–283.
- Liu, Y., Müller, S., Berger, D., Jelic, J., Reuter, K., Tonigold, M., Sanchez-Sanchez, M., and Lercher, J.A. (2016). Formation mechanism of the first carbon-carbon bond and the first olefin in the methanol conversion into hydrocarbons. Angew. Chem. Int. Ed. Engl. 55, 5723–5726.
- Chowdhury, A.D., Houben, K., Whiting, G.T., Mokhtar, M., Asiri, A.M., Al-Thabaiti, S.A., Basahel, S.N., Baldus, M., and Weckhuysen, B.M. (2016). Initial carbon-carbon bond formation during the early stages of the methanol-to-olefin process proven by zeolite-trapped acetate and methyl acetate. Angew. Chem. Int. Ed. Engl. 55, 15840– 15845.
- Wu, X., Xu, S., Zhang, W., Huang, J., Li, J., Yu, B., Wei, Y., and Liu, Z. (2017). Direct mechanism of the first carbon-carbon bond formation in the methanol-to-hydrocarbons process. Angew. Chem. Int. Ed. Engl. 56, 9039–9043.
- Wang, W., Jiao, J., Jiang, Y., Ray, S.S., and Hunger, M. (2005). Formation and decomposition of surface ethoxy species on acidic zeolite. Y. ChemPhysChem 6, 1467– 1469.
- Chowdhury, A.D., Lucini Paioni, A.L., Whiting, G.T., Fu, D., Baldus, M., and Weckhuysen, B.M. (2019). Unraveling the homologation reaction sequence of the zeolite-catalyzed ethanol-tohydrocarbons process. Angew. Chem. Int. Ed. Engl. 58, 3908–3912.
- Zhou, X., Wang, C., Chu, Y., Xu, J., Wang, Q., Qi, G., Zhao, X., Feng, N., and Deng, F. (2019). Observation of an oxonium ion intermediate in ethanol dehydration to ethene on zeolite. Nat. Commun. 10, 1961.





- Murray, D.K., Chang, J.W., and Haw, J.F. (1993). Conversion of methyl halides to hydrocarbons on basic zeolites: a discovery by in situ NMR. J. Am. Chem. Soc. 115, 4732–4741.
- Zhang, W., Zhang, M., Xu, S., Gao, S., Wei, Y., and Liu, Z. (2020). Methylcyclopentenyl cations linking initial stage and highly efficient stage in methanol-to-hydrocarbon process. ACS Catal 10. 4510–4516.
- Lesthaeghe, D., Van Speybroeck, V., Marin, G.B., and Waroquier, M. (2006). Understanding the failure of direct C-C coupling in the zeolitecatalyzed methanol-to-olefin process. Angew. Chem. Int. Ed. Engl. 45, 1714–1719.
- Lesthaeghe, D., Van Speybroeck, V., Marin, G.B., and Waroquier, M. (2006). What role do oxonium ions and oxonium ylides play in the ZSM-5 catalysed methanol-to-olefin process? Chem. Phys. Lett. 417, 309–315.
- 31. Lesthaeghe, D., Van Speybroeck, V., Marin, G.B., and Waroquier, M. (2007). The rise and fall of direct mechanisms in methanol-to-olefin catalysis: an overview of theoretical contributions. Ind. Eng. Chem. Res. 46, 8832–8838

- Müller, S., Liu, Y., Kirchberger, F.M., Tonigold, M., Sanchez-Sanchez, M., and Lercher, J.A. (2016). Hydrogen transfer pathways during zeolite catalyzed methanol conversion to hydrocarbons. J. Am. Chem. Soc. 138, 15994– 16003.
- 33. Brauman, J.I., Dodd, J.A., and Han, C. (1987). Intrinsic nucleophilicity. Advances in Chemistry 215, 23–33.
- Chen, X., and Brauman, J.I. (2008). Hydrogen bonding lowers intrinsic nucleophilicity of solvated nucleophiles. J. Am. Chem. Soc. 130, 15038–15046.
- Plessow, P.N., and Studt, F. (2017). Unraveling the mechanism of the initiation reaction of the methanol to olefins process using ab initio and dft calculations. ACS Catal 7, 7987–7994.
- Plessow, P.N., Smith, A., Tischer, S., and Studt, F. (2019). Identification of the reaction sequence of the MTO initiation mechanism using ab initio-based kinetics. J. Am. Chem. Soc. 141, 5908–5915.
- Wang, X., Wu, Q., Chen, C., Pan, S., Zhang, W., Meng, X., Maurer, S., Feyen, M., Müller, U., and Xiao, F.S. (2015). Atom-economical synthesis of

- a high silica CHA zeolite using a solvent-free route. Chem. Commun. (Camb) *51*, 16920–16923.
- Marcos-Alcalde, I., Setoain, J., Mendieta-Moreno, J.I., Mendieta, J., and Gómez-Puertas, P. (2015). MEPSA: minimum energy pathway analysis for energy landscapes. Bioinformatics 31, 3853–3855.
- Rybicki, M., and Sauer, J. (2018). Ab initio prediction of proton exchange barriers for alkanes at Brønsted sites of zeolite H-MFI. J. Am. Chem. Soc. 140, 18151–18161.
- Goncalves, T.J., Plessow, P.N., and Studt, F. (2019). On the accuracy of density functional theory in zeolite catalysis. ChemCatChem 11, 4368-4376.
- Sauer, J. (2019). Ab initio calculations for molecule-surface interactions with chemical accuracy. Acc. Chem. Res. 52, 3502–3510.
- Pidko, E.A. (2017). Toward the balance between the reductionist and systems approaches in computational catalysis: model versus method accuracy for the description of catalytic systems. ACS Catal 7, 4230–4234.

## **Supplemental information**

The first carbon-carbon bond formation mechanism in methanol-to-hydrocarbons process over chabazite zeolite

Tantan Sun, Wei Chen, Shutao Xu, Anmin Zheng, Xinqiang Wu, Shu Zeng, Nan Wang, Xiangju Meng, Yingxu Wei, and Zhongmin Liu

## **Table of Contents**

Supplemental Figure S1 XRD pattern of HSSZ-13	2
Supplemental Figure S2 SEM image of HSSZ-13	3
<b>Supplemental Figure S3</b> Effluent products at the initial MTH reaction stage at 300 °	C4
Supplemental Figure S4 <sup>13</sup> C CP MAS NMR spectrum for detection of SES	5
Supplemental Figure S5 2D <sup>13</sup> C- <sup>13</sup> C INADEQUATE spectrum for conformation of S	SES6
Supplemental Figure S6 The formation of TMO starting from DME and SMS	7
<b>Supplemental Figure S7</b> Effluent products at the initial MTH reaction stage at 220 °	C8
Supplemental Figure S8 AIMD simulations for the C-C bond formation start	ng from
methanol and SMS	9
Supplemental Figure S9 AIMD simulations for the C-C bond formation start	ng from
methanol and TMO.	10
Supplemental Figure S10 AIMD simulations for the C-C bond formation starting fr	om DME
and TMO	11
Supplemental Figure S11 The free energy profiles of the reaction process of ethano	or MEE
to ethene	12
Supplemental Figure S12 AIMD simulations for the C-C bond formation starting fi	om SMS
and CO	13
Supplemental Figure S13 Schematic of the two CVs	14
Supplemental Figure S14 The fitting relationships of potential energies between	PBE and
B3LYP methods	15
Supplemental Figure S15 Proposed reaction pathways for the methane formation	16
Supplemental Figure S16 In situ DRIFT spectra of methanol conversion	17
Supplemental Tables	18
Supplemental Notes	20
Supplemental References	27

## **Supplemental Figures**

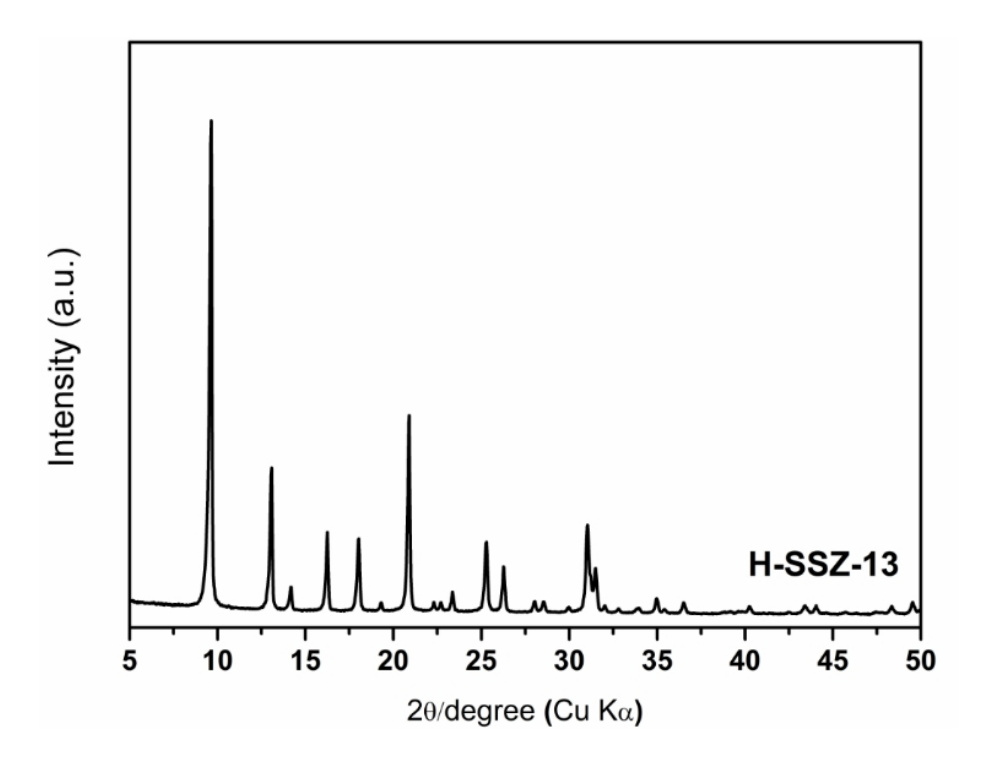


Figure S1. XRD pattern of HSSZ-13.

The XRD pattern of the fresh HSSZ-13 zeolite catalyst.

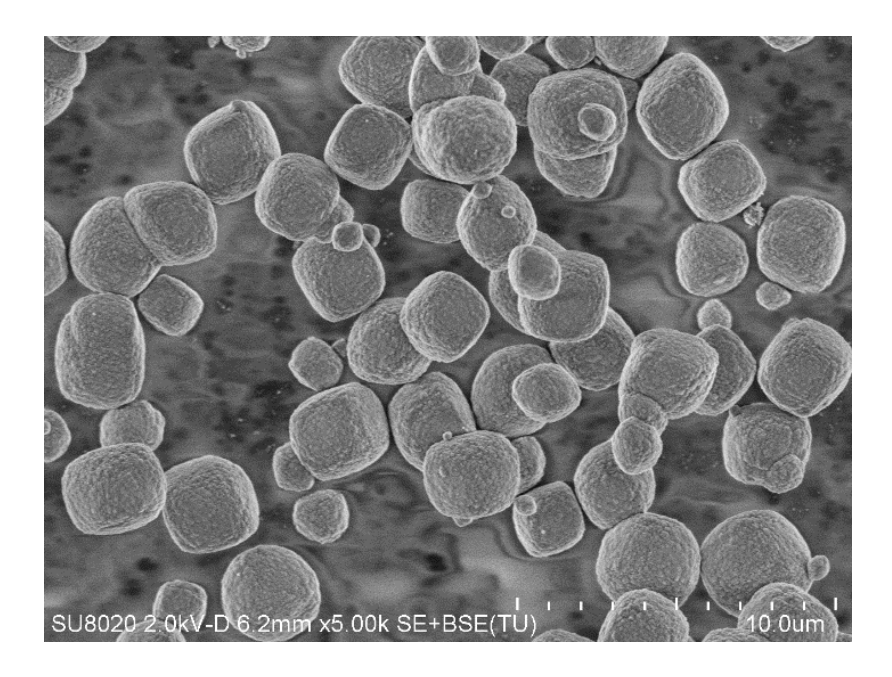


Figure S2. SEM image of HSSZ-13.

The SEM image of the fresh HSSZ-13.

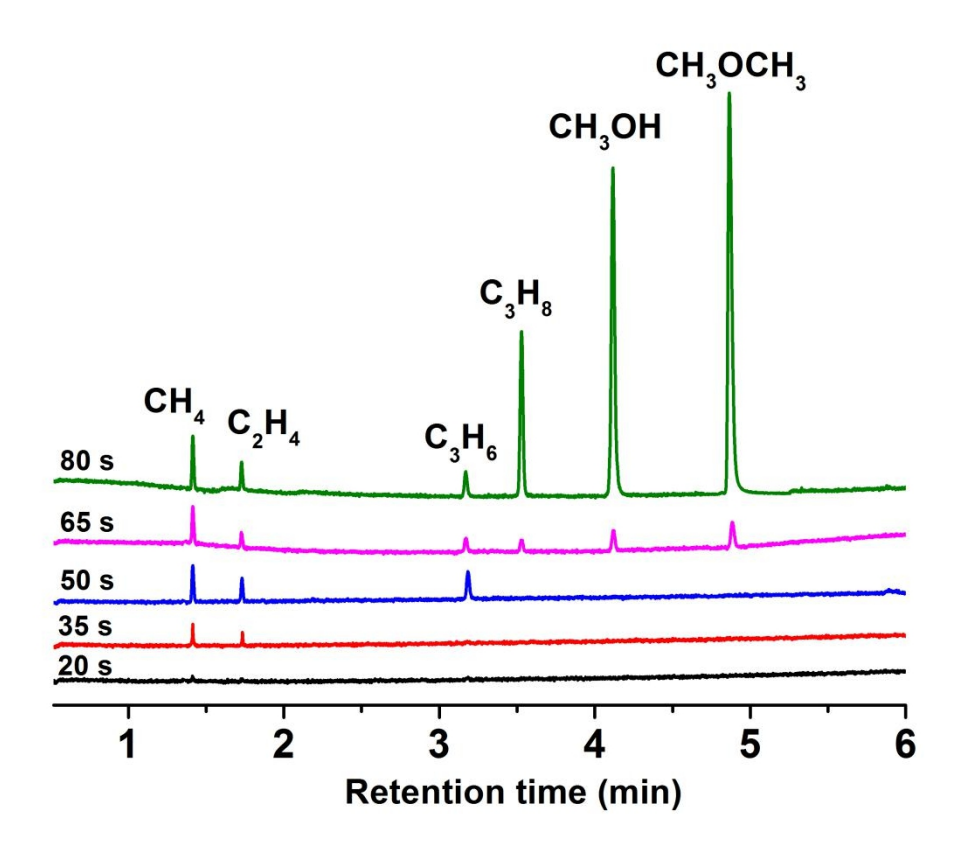


Figure S3. Effluent products at the initial MTH reaction stage at 300 °C.

The GC chromatograms of effluent products from the MTH reaction at 300  $^{\circ}$ C over the HSSZ-13 catalyst with a WHSV of 2  $h^{-1}$ .

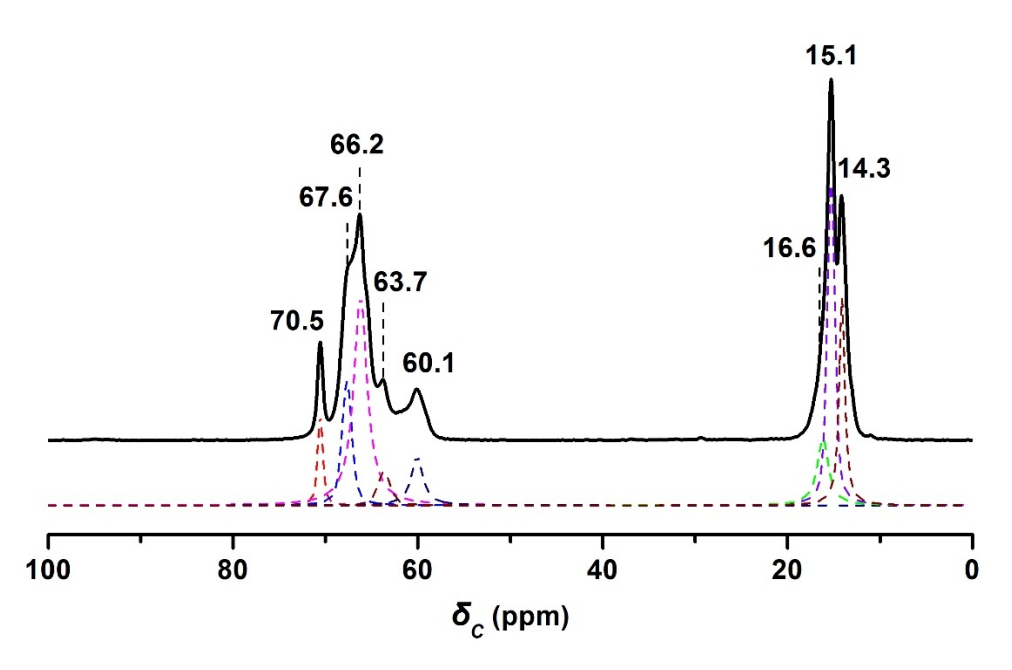


Figure S4. <sup>13</sup>C CP MAS NMR spectrum for detection of SES.

The  $^{13}C$  CP MAS NMR spectrum of HSSZ-13 after  $^{13}C_2$ -ethanol dehydrated at 150 °C for 1 h.

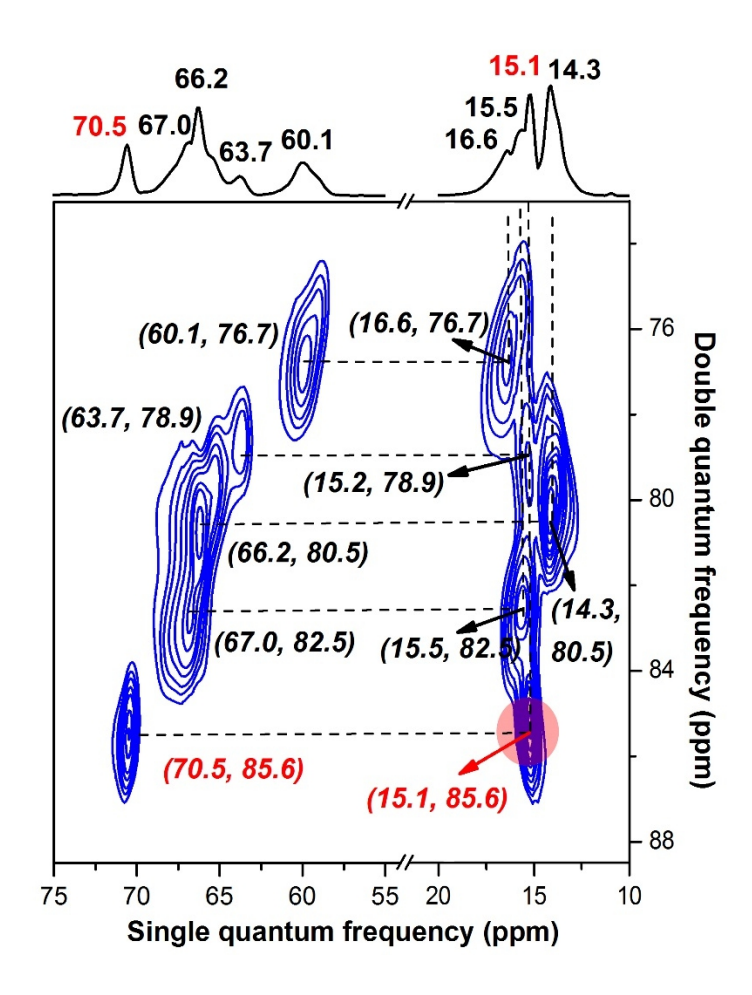


Figure S5. 2D <sup>13</sup>C-<sup>13</sup>C INADEQUATE spectrum for conformation of SES.

The 2D  $^{13}$ C- $^{13}$ C refocused INADEQUATE spectrum of HSSZ-13 after  $^{13}$ C<sub>2</sub>-ethanol dehydrated at 150 °C for 1 h.

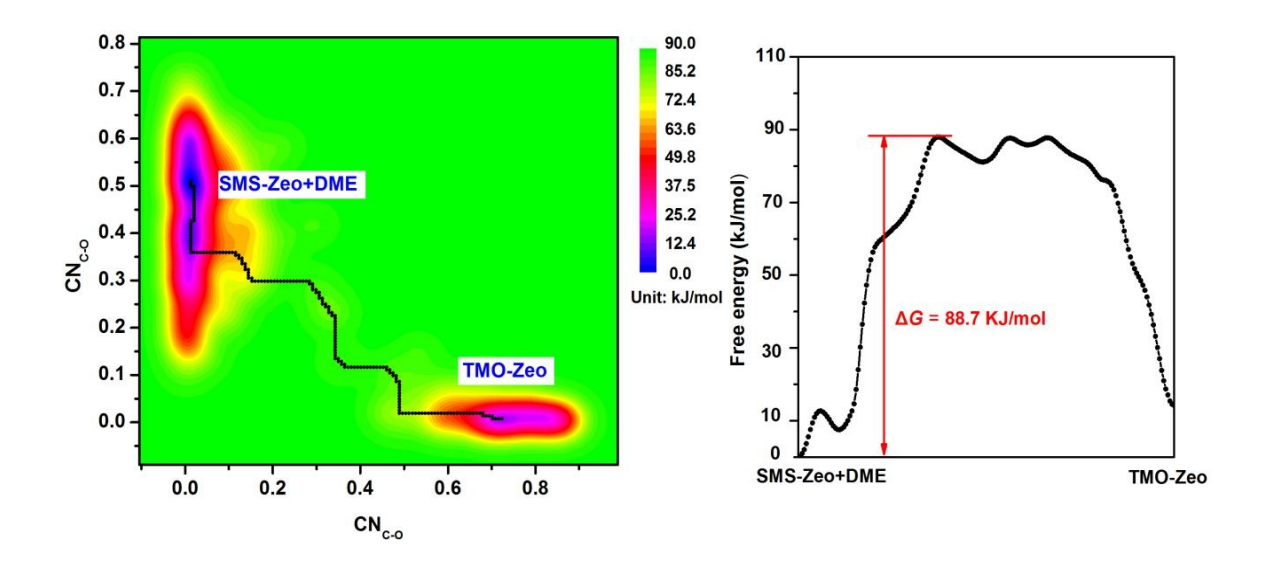


Figure S6. The formation of TMO starting from DME and SMS.

The 2D free energy surface and minimal energy path of TMO formation starting from DME and SMS (left) and free energy profiles along the minimal energy path (right).

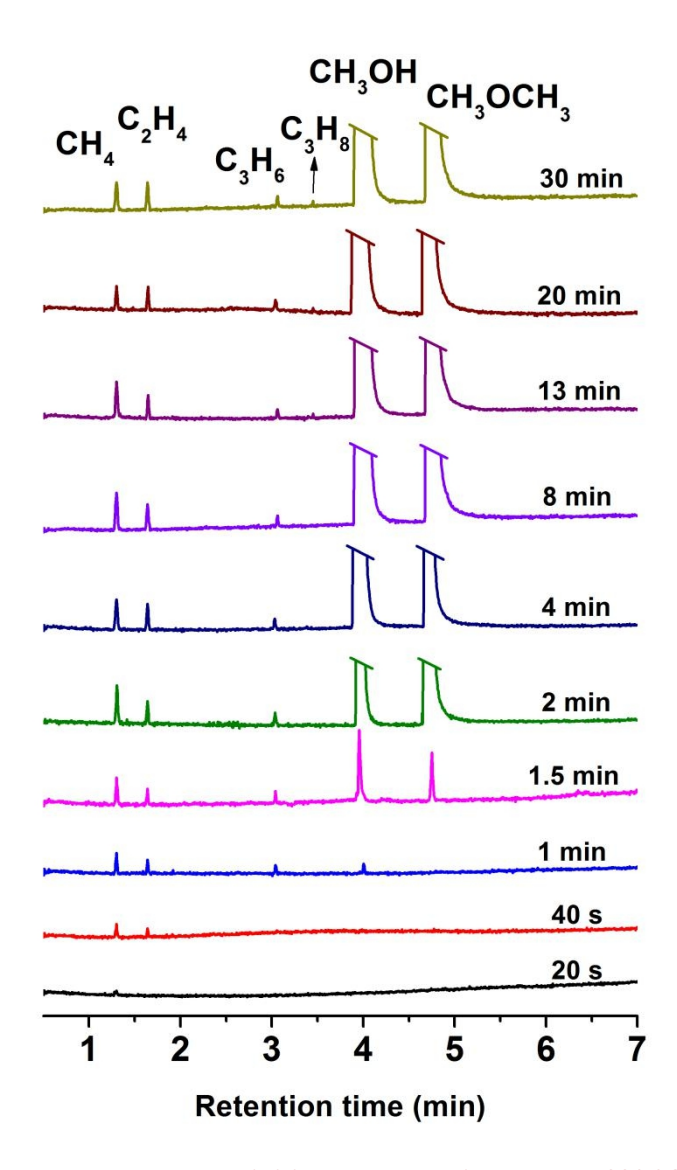


Figure S7. Effluent products at the initial MTH reaction stage at 220 °C.

The GC chromatograms of effluent products from the MTH reaction at 220  $^{\circ}$ C over the HSSZ-13 catalyst with a WHSV of 2  $h^{-1}$ .

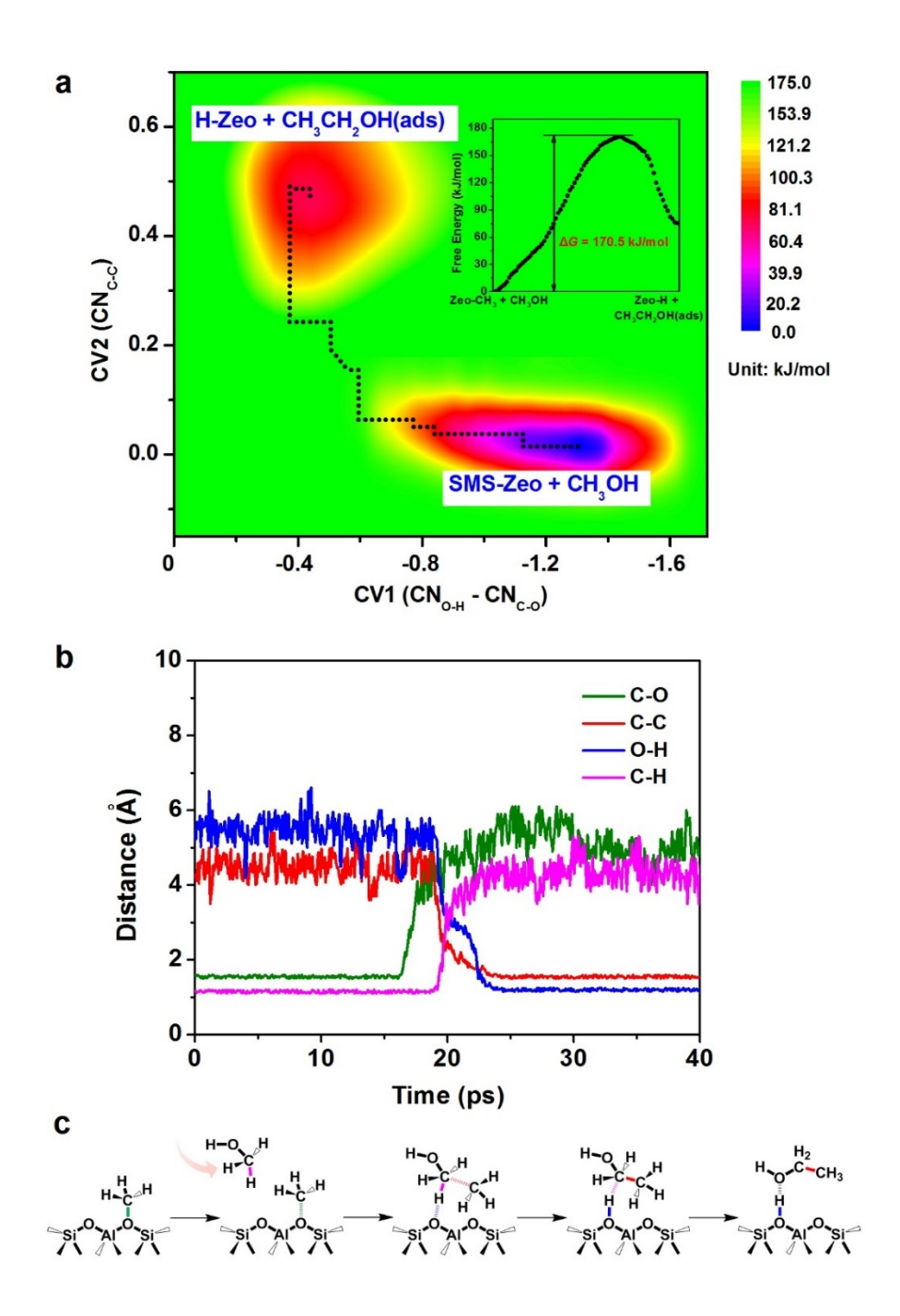


Figure S8. AIMD simulations for the C-C bond formation starting from methanol and SMS.

(a) 2D free energy surface and minimal energy path of the first C-C bond formation starting from methanol and SMS (Insets: free energy profiles along with the minimal energy path). (b) The evolution of the C-O, C-C, O-H and C-H bond distances in the methanol and SMS over HSSZ-13 zeolite with AIMD simulations. (c) The reaction path of SMS-Zeo + CH<sub>3</sub>OH to C<sub>2</sub>H<sub>5</sub>OH(ads) + H-Zeo.

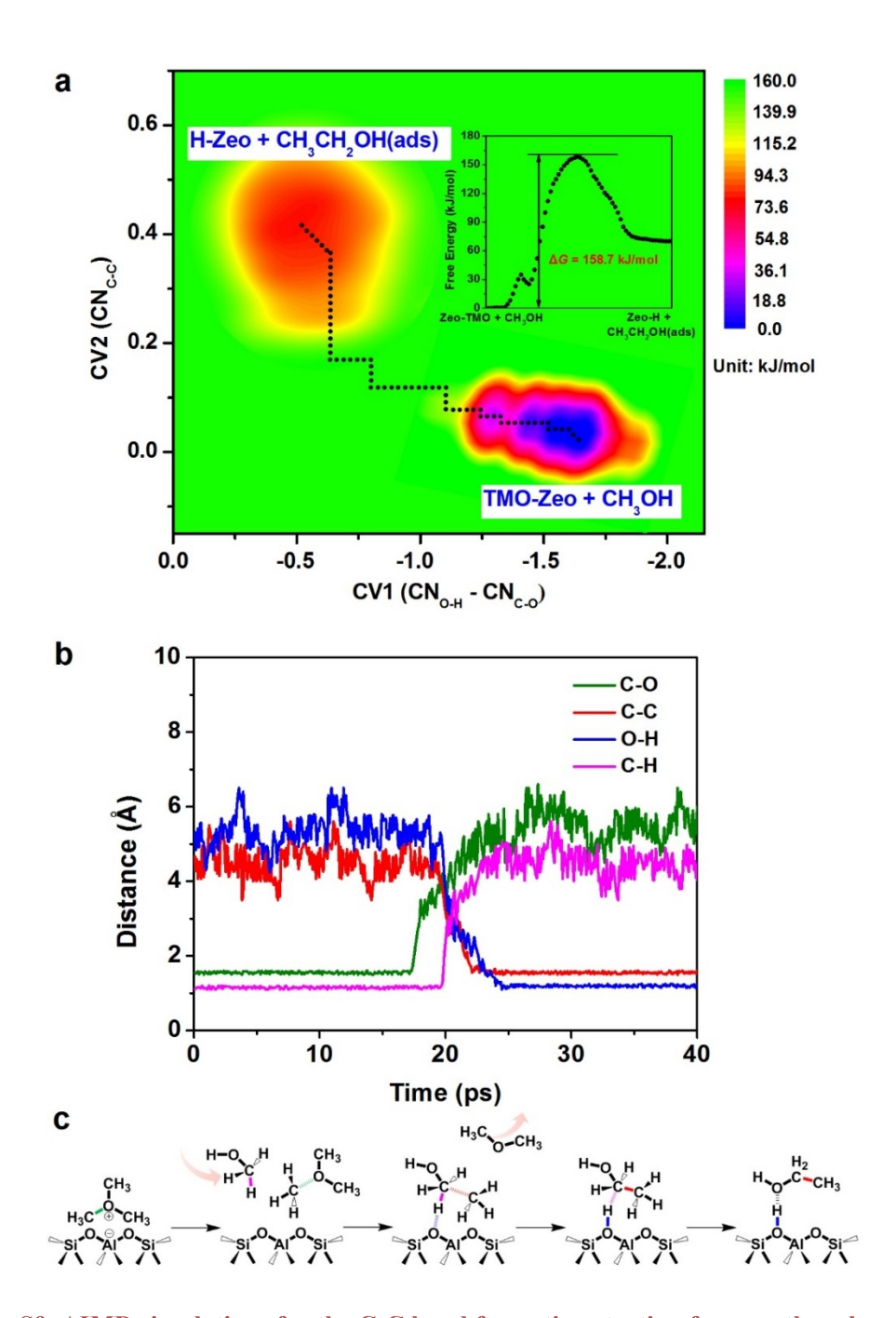


Figure S9. AIMD simulations for the C-C bond formation starting from methanol and TMO.

(a) 2D free energy surface and minimal energy path of the first C-C bond formation starting from methanol and TMO (Insets: free energy profiles along the minimal energy path). (b) The evolution of the C-O, C-C, O-H and C-H bond distances in the methanol and TMO over HSSZ-13 zeolite with AIMD simulations. (c) The reaction path of TMO-Zeo +  $CH_3OH$  to  $C_2H_5OH$ (ads) + H-Zeo.

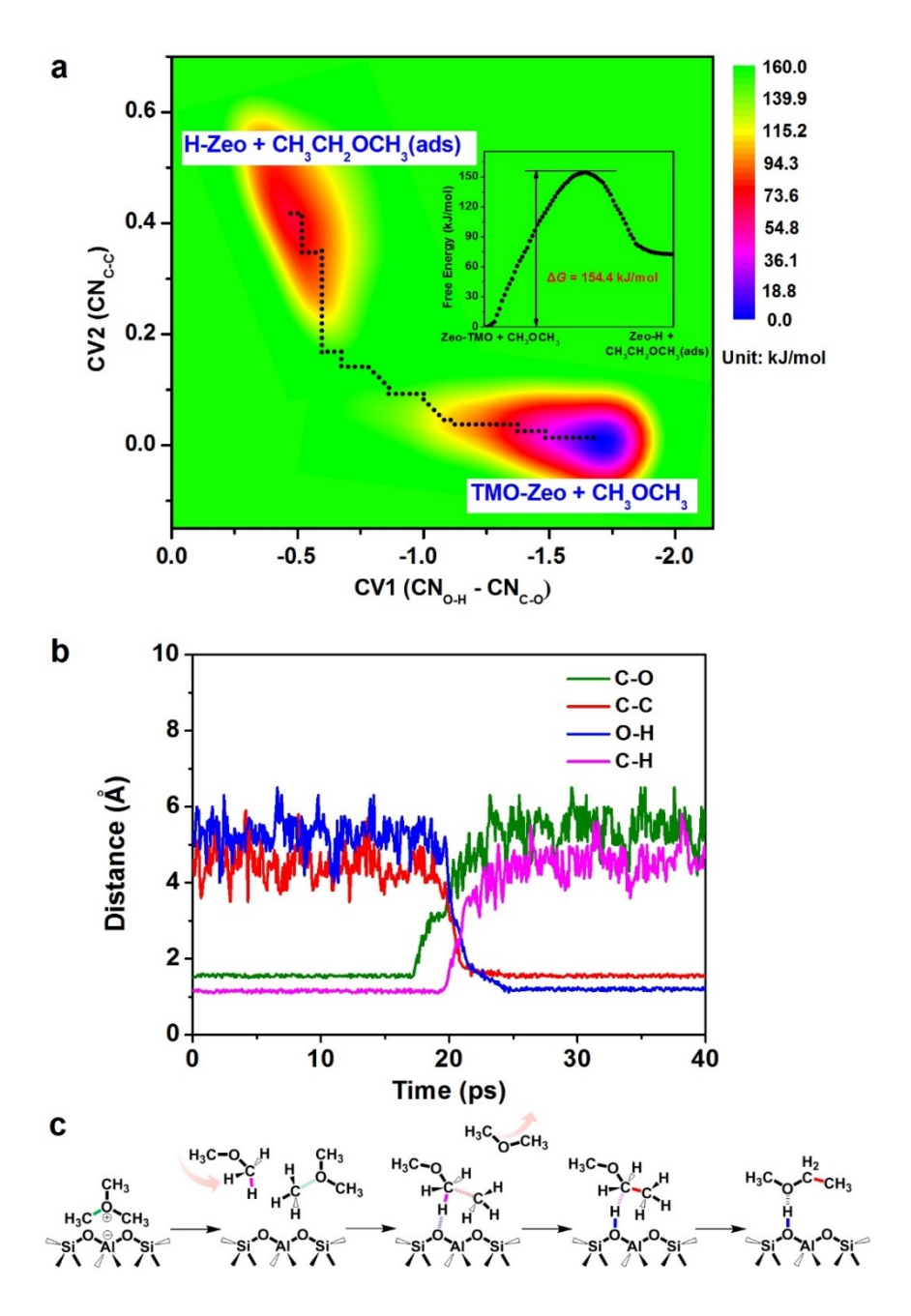


Figure S10. AIMD simulations for the C-C bond formation starting from DME and TMO.

(a) 2D free energy surface and minimal energy path of first C-C bond formation starting from DME and TMO (Insets: free energy profiles along the minimal energy path). (b) The evolution of the C-O, C-C, O-H and C-H bond distances in the DME and TMO over HSSZ-13 zeolite with AIMD simulations. (c) The reaction path of TMO-Zeo + CH<sub>3</sub>OCH<sub>3</sub> to C<sub>2</sub>H<sub>5</sub>OCH<sub>3</sub>(ads) + H-Zeo.

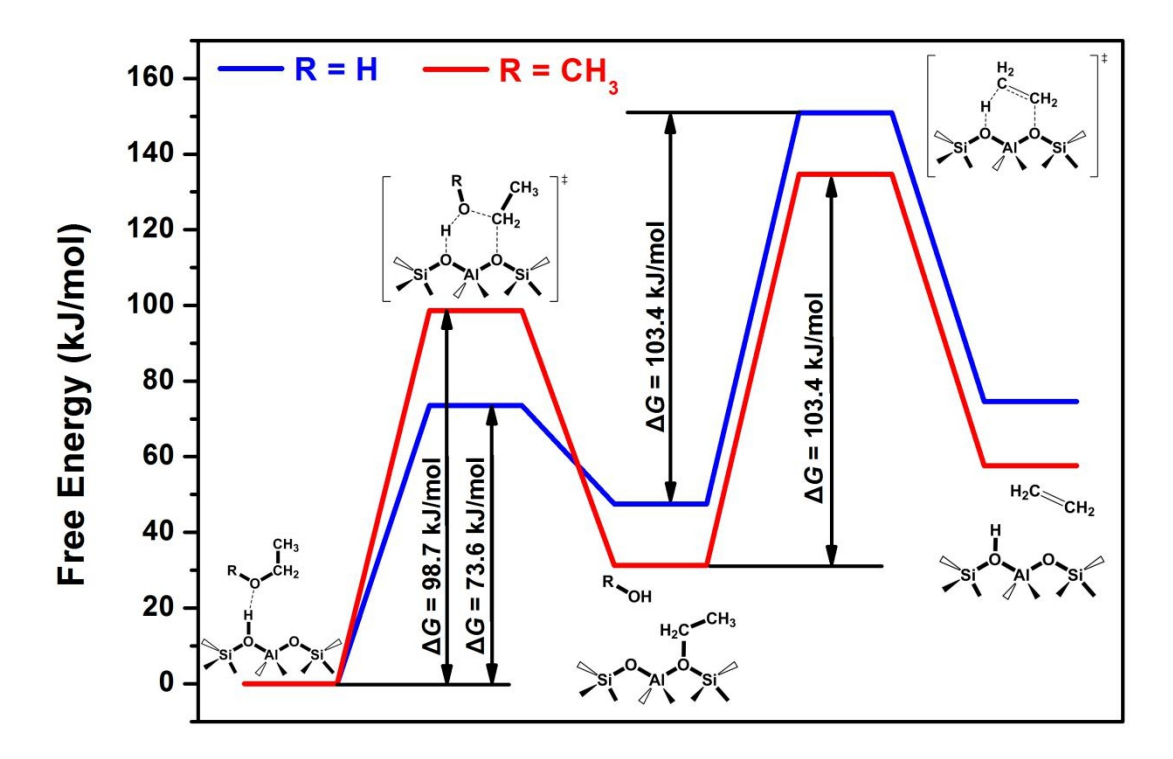


Figure S11. The free energy profiles of the reaction process of ethanol or MEE to ethene.

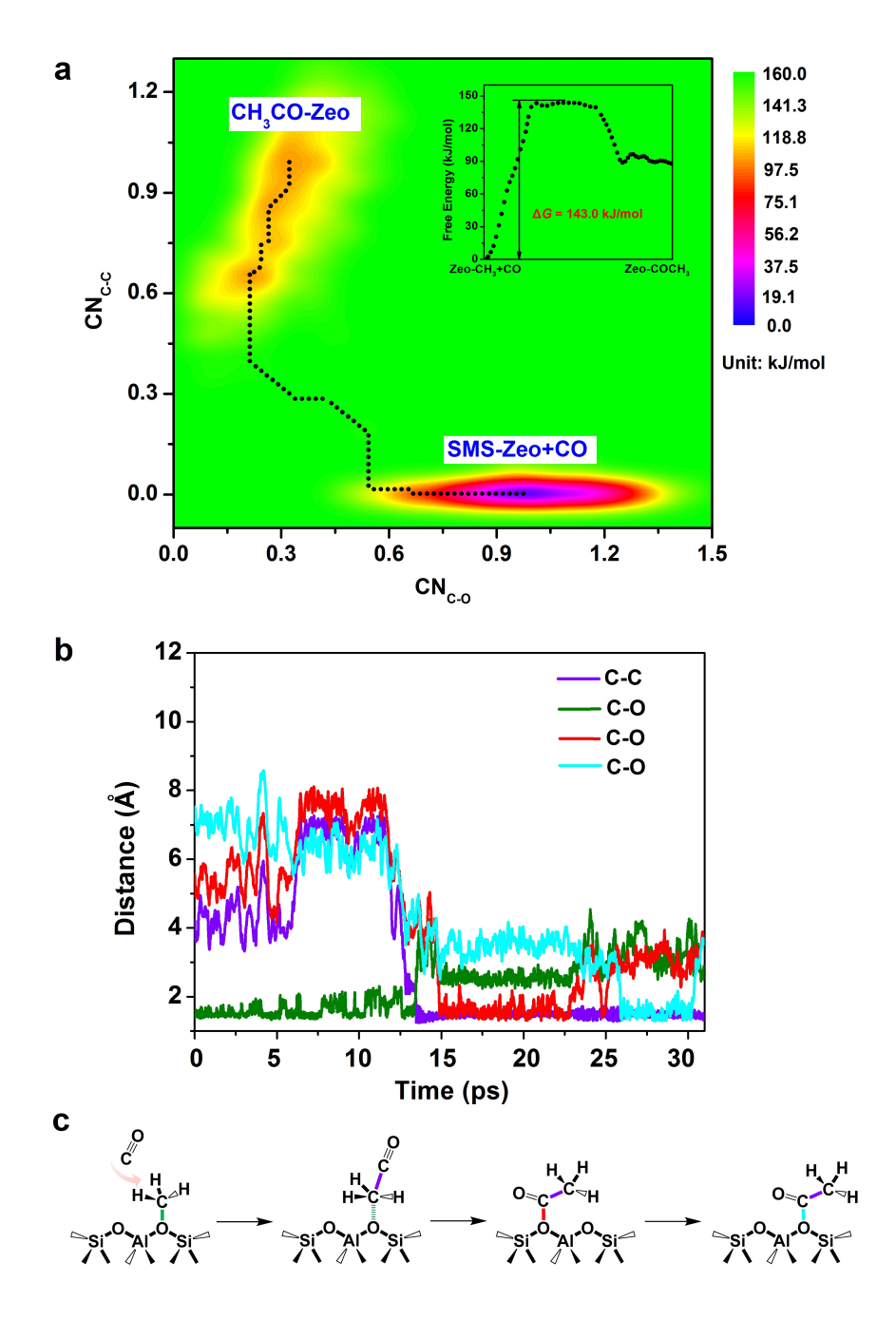


Figure S12. AIMD simulations for the C-C bond formation starting from SMS and CO.

(a) 2D free energy surface and minimal energy path of first C-C bond formation starting from SMS and CO (Insets: free energy profiles along the minimal energy path). (b) The evolution of the C-C and C-O bond distances in the SMS and CO over HSSZ-13 zeolite with AIMD simulations.

(c) The reaction path of SMS-Zeo + CO to CH<sub>3</sub>CO-Zeo.

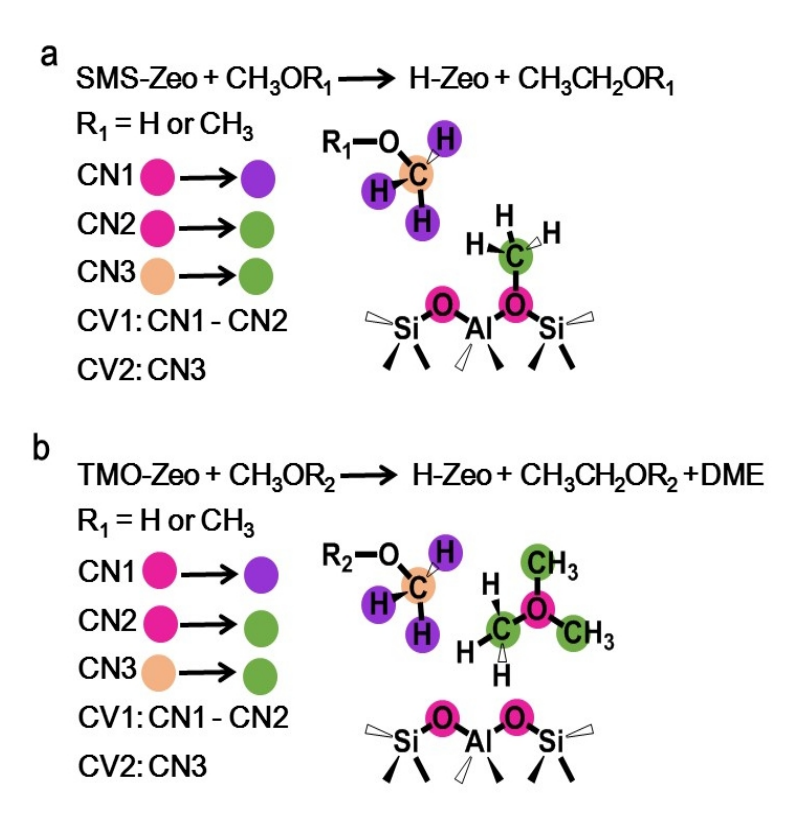


Figure S13. Schematic of the two CVs.

Schematic of the two Collective Variables (CV) applied during the meta-dynamics simulations of first C-C bond formation. (a) SMS-Zeo + CH<sub>3</sub>OR<sub>1</sub>, (b) TMO-Zeo +CH<sub>3</sub>OR<sub>2</sub>.

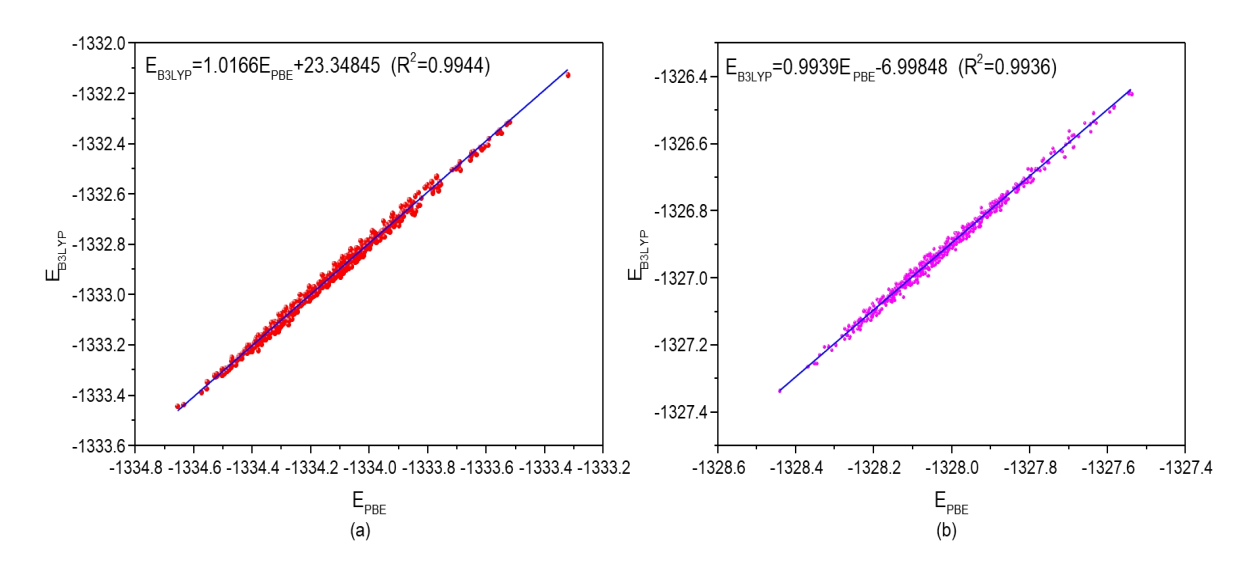


Figure S14. The fitting relationships of potential energies between PBE and B3LYP methods.

The fitting relationships of potential energies (in a.u.) between PBE and B3LYP methods for (a)

Path  $A_2$  (SSZ-13\_SMS + DME) and (b) Path  $A_1$  (SSZ-13\_SMS + methanol).

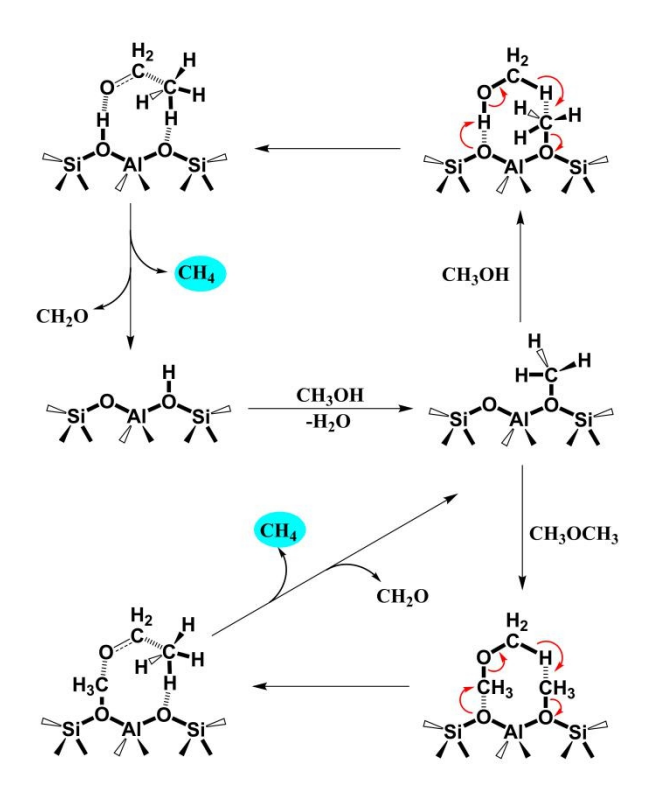


Figure S15. Proposed reaction pathways for the methane formation.

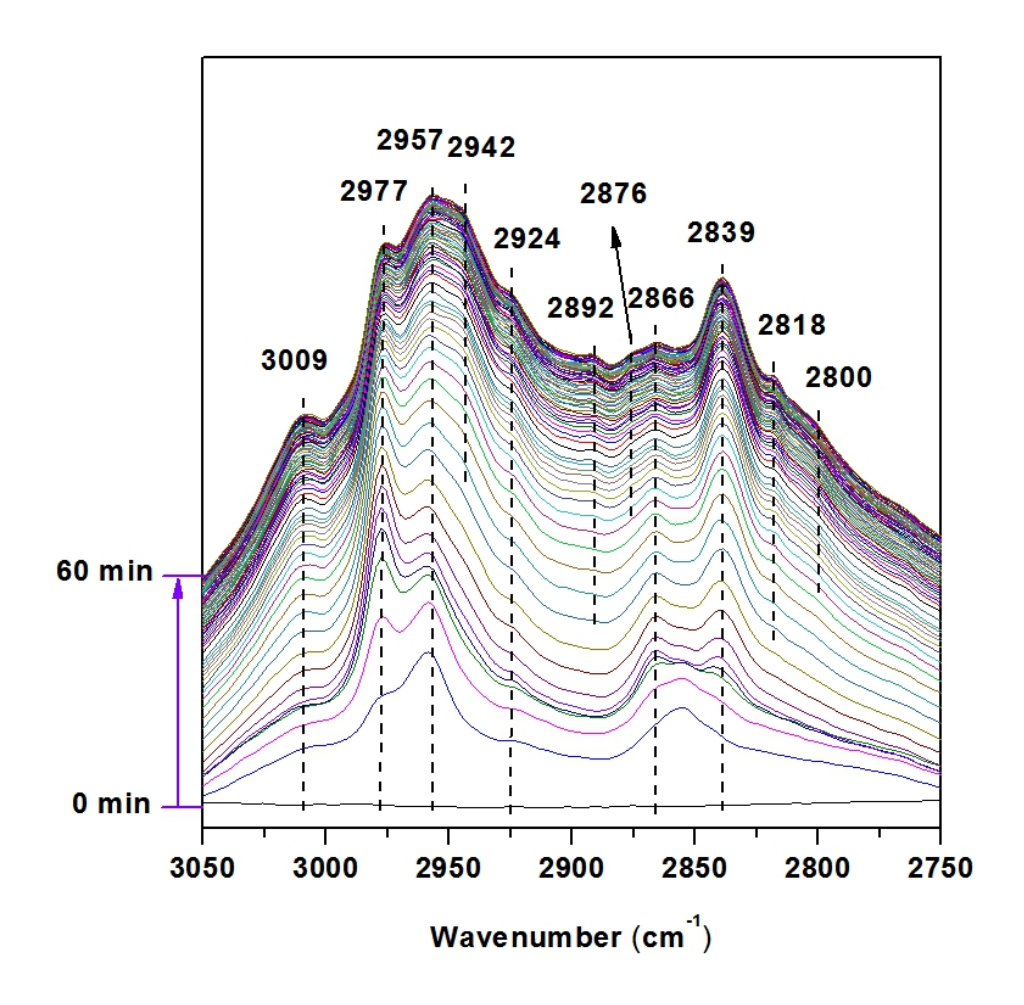


Figure S16. In situ DRIFT spectra of methanol conversion.

In situ DRIFT spectra in C-H stretching region recorded during methanol conversion over HSSZ-13 at 220 °C. The spectra were recorded every 60 s from 0 to 60 min.

### **Supplemental Tables**

**Table S1.** Basis sets test of DZVP, TZVP and TZV2P by the adsorption energies of DME and methanol on SSZ-13 with SMS.

Basis set	$\Delta E_{abs(DME)}kJ/mol$	$\Delta E_{abs(methanol)}kJ/mol$
DZVP	-77.6	-65.0
TZVP	-81.2	-75.9
TZV2P	-64.4	-53.0

**Table S2.** Comparison on adsorption energies of DME and methanol on SSZ-13 with SMS by revPBE-D3, PBEsol-D3, B3LYP-D3 and PBE0-D3 methods.

	revPBE-D3	PBEsol-D3	PBE-D3	B3LYP-D3	PBE0-D3
$\begin{array}{c} \Delta \; E_{abs(DME)} \\ kJ/mol \end{array}$	-56.8	-82.6	-77.6	-87.3	-80.5
$\begin{array}{c} \Delta \; E_{abs(methanol)} \\ kJ/mol \end{array}$	-47.8	-83.5	-65.0	-60.1	-54.1

**Table S3.** The thermodynamic parameters of DME, methanol and CO adsorption processes on SMS\_SSZ-13 and TMO\_SSZ-13.

SMS_SSZ-13	ΔE kJ/mol	ΔU kJ/mol	ΔH kJ/mol	ΔS J/mol/K	ΔG kJ/mol
DME	-77.6	-60.1	-65.7	-133.3	24.1
Methanol	-65.0	-47.8	-53.4	-118.3	26.3
CO	-35.8	-21.6	-27.2	-94.9	36.7
TMO_SSZ-13	ΔE kJ/mol	ΔU kJ/mol	ΔH kJ/mol	ΔS J/mol/K	ΔG kJ/mol
DME	-100.8	-82.6	-88.2	-135.2	2.8
Methanol	-89.8	-71.8	-77.3	-133.6	12.6

Table S4. Free energy barriers (in kJ/mol) of the first C-C bond formation by SMS + methanol,  $SMS + methanol, TMO + methanol, TMO + DME \ and \ SMS + CO. \ (Where \ \Delta G_{ads}, \ \Delta G_{int} \ and \ \Delta G_{app}$  are adsorption free energies, intrinsic free energy barriers and apparent free energy barriers

respectively,  $\Delta G_{app} = \Delta G_{ads} + \Delta G_{int}$ )

Reactants	$\Delta G_{ads}$	$\Delta G_{int}$	$\Delta G_{app}$
SMS + methanol	26.3	170.5	196.8
SMS + DME	24.1	141.6	165.7
TMO + methanol	12.6	158.7	171.3
TMO + DME	2.8	154.4	157.2
SMS + CO	36.7	143.0	179.7

**Table S5.** The rotational, translational, vibrational and electronic contributions to entropy (S, in J/mol/K) and entropy change ( $\Delta$ S) at 673K for the process of methanol adsorbed on SMS\_SSZ-13

	$S_{total}$		$S_{rotation}$		$S_{translation}$		$S_{vibration}$	
	all	8T	all	8T	all	8T	all	8T
Methanol	28	5.8	8	9.8	16	59.0	27	7.1
SMS_SSZ-13	3147.2	837.2	193.8	193.8	220.1	220.1	2733.4	423.4
SMS_SSZ-13_Methanol	3314.7	998.5	193.8	193.8	220.3	220.3	2900.7	584.5
ΔS	-118.3	-124.5	-89.7	-89.8	-168.8	-168.8	140.3	134.0

#### **Supplemental Notes**

#### **Supplemental Note 1**

Initial MTH reaction over HSSZ-13 at 300 °C. Methanol conversion over HSSZ-13 at 300 °C with time on stream (TOS) less than 80 s were monitored by an online gas chromatography. From Figure S3, the feeding of methanol for the first 20 s only generated a trace amount of methane. However, upon continuous feeding of methanol, up to 35 to 50 s, ethene and propene were detected apart from methane. When the feeding of methanol continued more than 65 s, methanol and DME were captured. The absence of methanol and DME for the first 65 s implied that the initially fed methanol and its dehydrated product DME stayed on the surface of the HSSZ-13 as strongly adsorbed species until methanol was in excess. The initially-formed hydrocarbons, especially ethene, which is the compound with a C-C bond during this period, was speculated to derive from the conversion of the adsorbed species on the surface of HSSZ-13. Ethene detection ahead of the release of the reactants indicated that the direct conversion of surface-adsorbed/bound species, such as methanol, DME, SMS, and some other C1 species, should be responsible for the formation of the initial hydrocarbons with C-C bond.

#### **Supplemental Note 2**

Initial MTH reaction over HSSZ-13 at 220 °C. Methanol conversion over HSSZ-13 at 220 °C with time on stream (TOS) less than 30 min were monitored by an online gas chromatography. From Figure S7, the feeding of methanol for the first 20 s only generated a trace amount of methane. However, upon continuous feeding of methanol, up to 40 s, ethene was detected apart from methane. When methanol was fed for 60 s propene and methanol appeared in gas effluent.

Similar to the results of MTH reaction at 300 °C (Figure S3), ethene was detected ahead of the appearance of methanol and DME in effluent. Moreover, as a MTH product generated by hydrogen transfer reaction of initially-formed olefinic species, propane was detected at the period of 13 to 30 min.

#### **Supplemental Note 3**

Surface ethoxy species (SES) on HSSZ-13. In Figure S4, the peaks at 70.5 ppm is attributed to methylene carbon atom of surface ethoxy species (SES), formed by ethanol adsorption and dehydration on the Brønsted acid site (BAS). Signals at 60.1 and 63.7 ppm are originated from  $\alpha$  carbon atom of ethanol with different adsorption state<sup>1</sup>. Meanwhile, peaks at 66.2 and 67.6 ppm are attributed to  $\alpha$  carbon atom of diethyl ether (DEE) with different adsorption state<sup>1,2</sup>. Peaks at the range of 10 to 20 ppm are attributed to methyl carbon atoms of SES, ethanol and DEE.

#### **Supplemental Note 4**

2D <sup>13</sup>C-<sup>13</sup>C **refocused INADEQUATE spectrum.** To further confirm the 1D <sup>13</sup>C NMR assignment of SES in Figure S4, 2D <sup>13</sup>C-<sup>13</sup>C refocused INADEQUATE was recorded and presented in Figure S5. In this *J*-based experiment, two directly bonded <sup>13</sup>C share a common frequency in the F1 (vertical) dimension at the sum of their <sup>13</sup>C individual frequencies in the F2 (horizontal) dimension<sup>3</sup>. The cross-peak observed in the INADEQUATE spectrum notably allowed us to explicitly identified the methylene and methyl carbon atom of SES. From Figure S5, the SES can be identified through correlations between methylene carbon atom (70.5 ppm) and methyl carbon atom (15.1 ppm).

#### **Supplemental Note 5**

The reliability of DZVP basis set and PBE-D3 method. The reliability of DZVP basis set and PBE-D3 method has been tested by the DME/methanol adsorption energies on SSZ-13 with SMS, and we further estimate the error on energy barrier between PBE-D3 and B3LYP-D3 by the established relationship. All adsorption structures of DME or methanol on SSZ-13 with SMS were optimized to the minimum at different functional and basis sets. As listed in Table S1, the adsorption energies of DME and methanol by DZVP basis set are among the result of TZVP basis set and TZV2P basis set with the deviation of 3.6 ~ 13.2 kJ/mol, which indicates the reliability of DZVP basis set used in this work. Furthermore, the reliability of PBE-D3 method was also tested by the adsorption energies of DME and methanol, we employed two variants of PBE-D3 (revPBE-D3 and PBEsol-D3) and two hybrid functional (B3LYP-D3 and PBE0-D3) to calculate the adsorption as the comparison to PBE-D3. As listed in Table S2, revPBE-D3 significantly underestimate the adsorption energies by comparing with two hybrid functional, and PBEsol-D3 even predict the higher adsorption energy of methanol than DME. There is consistence in the results between PBE-D3 and two hybrid functional with the small deviation of  $2.9 \sim 10.9$  kJ/mol. To estimate the deviation between PBE-D3 and B3LYP-D3, we also randomly extracted 550 structures from the reaction process of AIMD simulations to calculate their potential energies by both PBE-D3 and B3LYP-D3 methods. According to these energies, there is an excellent linear relationship between two methods for C-C bond formation in SSZ-13\_SMS + DME and SSZ-13 SMS + methanol. During the energy barrier calculations, the deviation between PBE-D3 and B3LYP-D3 only depend on the slope of these linear relationships (Figure S14). The energy

barriers of the first C-C bond formation would change from 141.6 kJ/mol (Path A<sub>2</sub>) and 170.5 kJ/mol (Path A<sub>1</sub>) of PBE-D3 to 144.0 kJ/mol (Path A<sub>2</sub>) and 169.5 kJ/mol (Path A<sub>1</sub>) of B3LYP-D3 respectively. It can be concluded that the combination of functional and basis set in this work is accurately enough to calculate the first C-C bond formation in HSSZ-13 by comparing with hybrid functional and bigger basis set.

#### **Supplemental Note 6**

Free energy barriers with the consideration of adsorption. Moreover, the current free energy barriers in Figure 5 are the intrinsic free energy barriers (ΔG<sub>int</sub>). If the adsorption Gibbs free energy ( $\Delta G_{ads}$ ) was involved to reveal the apparent free energy barriers ( $\Delta G_{app}$ , the thermodynamic parameters of methanol/DME/CO adsorbed in HSSZ-13 with SMS or TMO were listed in Table S3), the corresponding  $\Delta G_{app}$  were 196.8, 165.7, 171.3, 157.2 and 179.7 kJ/mol for C-C bond formation via SMS + methanol, SMS + DME, TMO + methanol TMO + DME and SMS + CO respectively (Table S4). Notably, the free energy barriers of the first C-C formation have included the entropic effect with the fully consideration of anharmonic effect by AIMD simulations, but the entropies of adsorption process in Table S3 were obtained by harmonic frequency calculations without consideration the anharmonic effect, which may result some deviations to obtain more accurate  $\Delta G$  of adsorption process. Note that the thermodynamic calculations to entropy and Gibbs free energy in this work include the vibrational modes of all framework atoms, but a lot of small frequencies of framework atom vibrations might lead to the error on entropy calculations. It is better to calculate frequencies exclude the extra framework atoms to avoid the possible error. Here are the formulas to calculation entropy.

$$S_{translation} = R\left[\ln\left(\frac{RT}{N_A P}\left(\frac{2\pi m k T}{h^2}\right)^{3/2}\right) + \frac{5}{2}\right] \tag{1}$$

$$S_{rotation} = R \left[ ln \frac{8\pi^2 IkT}{\sigma h^2} + \frac{3}{2} \right]$$
 (2)

$$S_{vibration} = R \sum_{i} \left\{ \frac{h v_i}{kT} \frac{e^{-h v_i / (kT)}}{1 - e^{-h v_i / (kT)}} - \ln \left[ 1 - e^{-h v_i / (kT)} \right] \right\}$$
(3)

$$S_{total} = S_{translation} + S_{rotation} + S_{vibration}$$
 (4)

#### **Supplemental Note 7**

On the generation of methane at initial MTH stage. In this work, based on the experimental evidences and AIMD simulations, we established the complete direct first C-C bond formation pathway. In this direct mechanism, as shown in Figure 5, when SMS/TMO and the adjacent framework oxygen work together in an associative manner, the H atom of the DME/methanol would be donated to the negatively charged framework oxygen and a simultaneous methylation gives rise to a surface-adsorbed ethanol or MEE containing the first C-C bond. Then, SES will be generated by the transformation of the adsorbed ethanol or MEE. The generated SES, as ethene precursor, can be decomposed quickly, and finally the initial ethene will be eliminated from the catalyst surface. However, as shown in Figure S15, the electrophilic attack from SMS may lead to another option, in which the adjacent DME/methanol could donate its H atom to SMS, and in this way, the adduct of methane and adsorbed formaldehyde would be generated. In this case, methane and formaldehyde, especially methane, the inert product without strong adsorption on the zeolite catalyst, could be released into the gas phase as products.

In addition, for the formation of methane at the initial stage of MTH reaction, Venuto et al. and Haw et al. found that the abstraction of a hydride from methanol or hydrocarbon products by

SMS can result in the generation of methane.<sup>6</sup> Guo et al. found that at high temperature (> 350 °C), the decomposition reactions of methanol and DME were the main routes of methane formation, while at low temperature (< 350 °C) the hydrogenolysis reactions of methanol and DME for generating methane became principal.<sup>7</sup>

#### **Supplemental Note 8**

In situ DRIFT spectra of methanol conversion over HSSZ-13 at 220 °C. As presented in Figure S16, at the very beginning of methanol conversion, six absorbance bands appeared and their ascription are as follow: absorbance bands at 2977 and 2866 cm<sup>-1</sup> are attributed to stretching vibrations of C-H bond in SMS; absorbance bands at 2957 and 2924 cm<sup>-1</sup> belong to stretching vibrations of C-H bond in methanol; 3009 and 2839 cm<sup>-1</sup> are originated from stretching vibrations of C-H bond in DME.<sup>5,8</sup> However, upon continuous feeding of methanol, up to 12 min, new surface species with C-H absorbance bands at 2942, 2892, 2876, 2818 and 2800 cm<sup>-1</sup> are observed. These newly-formed species may attribute to surface hydrocarbons that generated by secondary reactions of the initially-formed olefin products.<sup>9,10</sup> The critical intermediates SES and surface methyleneoxy analogue (surface activated C1 species) that observed in NMR data were not successfully captured in our in situ DRIFT spectra. Moreover, according to document report, the stretching vibrations of C-H bond in -CH<sub>2</sub>- are at ca. 2940 and 2840 cm<sup>-1</sup>.<sup>11</sup> It could possible that the signals of SES may be overlapped by adsorbed methanol and DME.

#### **Supplemental Note 9**

Explanations for the loss of entropy of methanol after adsorption. From table S5, it can be

seen the entropy of gas phase methanol was significantly reduced in the adsorption process. We decomposed the total entropy and entropy change (at 298 K and 673 K) to rotational, translational and vibrational contributions as listed in Table S5 to explain this reason. The rotational and translational entropies (S<sub>rotation</sub> and S<sub>translation</sub>) before and after methanol adsorption nearly keep unchanged, but the vibrational entropies (S<sub>vibration</sub>) was hugely increased from 1306.2 J/mol/K to 1412.8 J/mol/K at 298 K and 2733.4 J/mol/K to 2900.7 J/mol/K at 673 K. Therefore, the vibrational contribution to entropy is responsible for the loss of methanol entropy during the adsorption process.

#### **Supplemental References**

- Chowdhury, A. D. et al. (2019). Unraveling the homologation reaction sequence of the zeolite-catalyzed ethanol-to-hydrocarbons process. Angew. Chem. Int. Ed. 58, 3908-3912.
- 2. Zhou, X. *et al.* (2019). Observation of an oxonium ion intermediate in ethanol dehydration to ethene on zeolite. Nat. Commun. *10*, 1961.
- 3. Xiao, D. *et al.* (2017). Direct structural identification of carbenium ions and investigation of host-guest interaction in the methanol to olefins reaction obtained by multinuclear NMR correlations. Chem. Sci. 8, 8309-8314.
- Wu, X. et al. (2017). Direct mechanism of the first carbon-carbon bond formation in the methanol-to-hydrocarbons process. Angew. Chem. Int. Ed. 56, 9039-9043.
- 5. Wu, X. *et al.* (2018). Evolution of C-C bond formation in the methanol-to-olefins process: from direct coupling to autocatalysis. ACS Catal. *8*, 7356-7361.
- Munson, E. et al. (1992). In situ solid-state NMR study of methanol-to-gasoline chemistry in zeolite HZSM-5. J. Phys. Chem. 96, 7740-7746.
- 7. Zhao, W. *et al.* (2014). Methane formation route in the conversion of methanol to hydrocarbons. J. Energy Chem. *23*, 201-206.
- 8. Campbell, S. *et al.* (1999). Methanol to hydrocarbons: spectroscopic studies and the significance of extra-framework aluminium. Micropor. Mesopor. Mat. *29*, 91-108.

- 9. Chen, J. *et al.* (1989). A transmission infrared spectroscopic investigation of the reaction of dimethyl ether with alumina surfaces. Langmuir *5*, 352-356.
- 10. Zhou, H. *et al.* (2015). Promotion effect of Fe in mordenite zeolite on carbonylation of dimethyl ether to methyl acetate. Catal. Sci. Tech. *5*, 1961-1968.
- Silverstein, R. et al. Spectrometric Identification of Organic Compounds [M]. John Wiley & Sons, Inc.